Chapter 6

Postbuckling response of functionally graded hybrid composite plates under combined uniaxial compression and in-plane shear loads

6.1. Introduction

The postbuckling response of functionally graded hybrid composite plates subjected to combined uniaxial and in-plane shear loading conditions is numerically investigated in the present study. The finite element formulation-based software ABAQUS has been used for the numerical study. Eigen buckling analysis and Tsai-Hill failure criterions are used to determine critical buckling and first ply failure loads, respectively. Functionally graded composite plates with and without cutouts are considered for the study. Five different shapes and three different sizes of cutouts at the center of the plate have been taken to examine the response under the combined in-plane loads. Effect of $(0/90)_{4s}$, $(+45/-45)_{4s}$, and $(+45/-45/0/90)_{2s}$ fiber stacking sequences are also examined. It is shown that, diamond-shaped cutout of small size among the cutouts performs better in terms of buckling and first ply failure loads of the plates under compressive loads combined with negative in-plane shear load. The $(+45/-45)_{4s}$ stacking sequence has the highest buckling and failure loads in comparison to other layup sequences.

Functionally graded hybrid composite plates modelled with and without cutouts and are numerically studied for their buckling, postbuckling response and first failure using ABAQUS. Furthermore, effect of load ratios on the postbuckling response is presented along with load-interaction curves. Schematics of functionally graded composite plates with different stacking sequences are shown in Fig. 6.1 for the study.

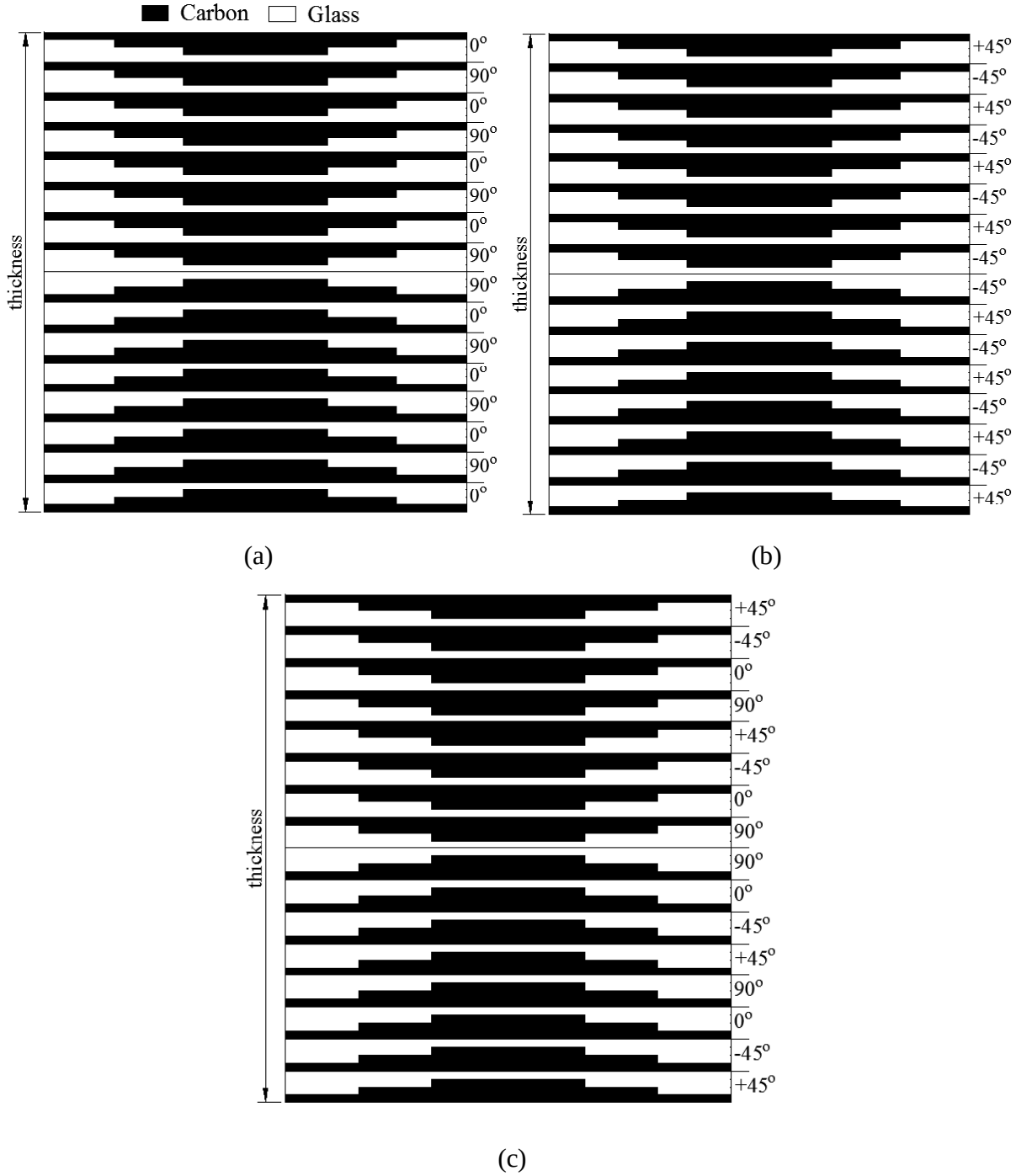

Fig. 6.1. Functionally graded hybrid plates held in thickness direction with fiber aligned in: (a) $(0/90)_{4s}$ direction; (b) $(+45/-45)_{4s}$ direction; (c) $(+45/-45/0/90)_{2s}$ direction

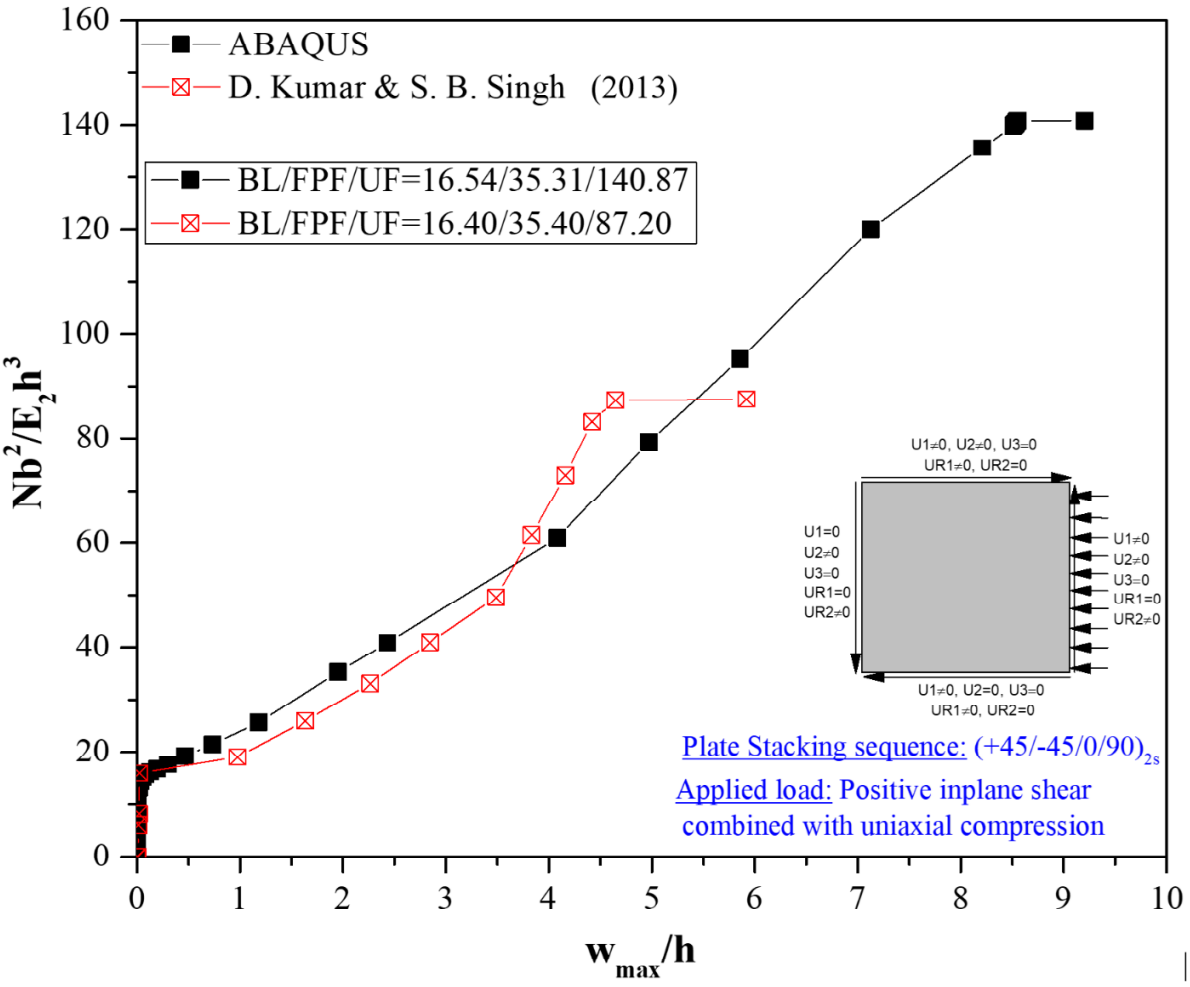
ABAQUS
D. Kumar & S. B. Singh (2013)
BL/FPF/UF=16.54/35.31/140.87
BL/FPF/UF=16.40/35.40/87.20
Nb^2/E_2h^3
w_{max}/h
U1≠0, U2≠0, U3=0
UR1≠0, UR2=0
U1=0
U2≠0
U3=0
UR1=0
UR2≠0
U1≠0
U2≠0
U3=0
UR1=0
UR2≠0
U1≠0, U2=0, U3=0
UR1≠0, UR2=0
Plate Stacking sequence: $(+45/-45/0/90)_{2s}$
Applied load: Positive inplane shear combined with uniaxial compression

(a)

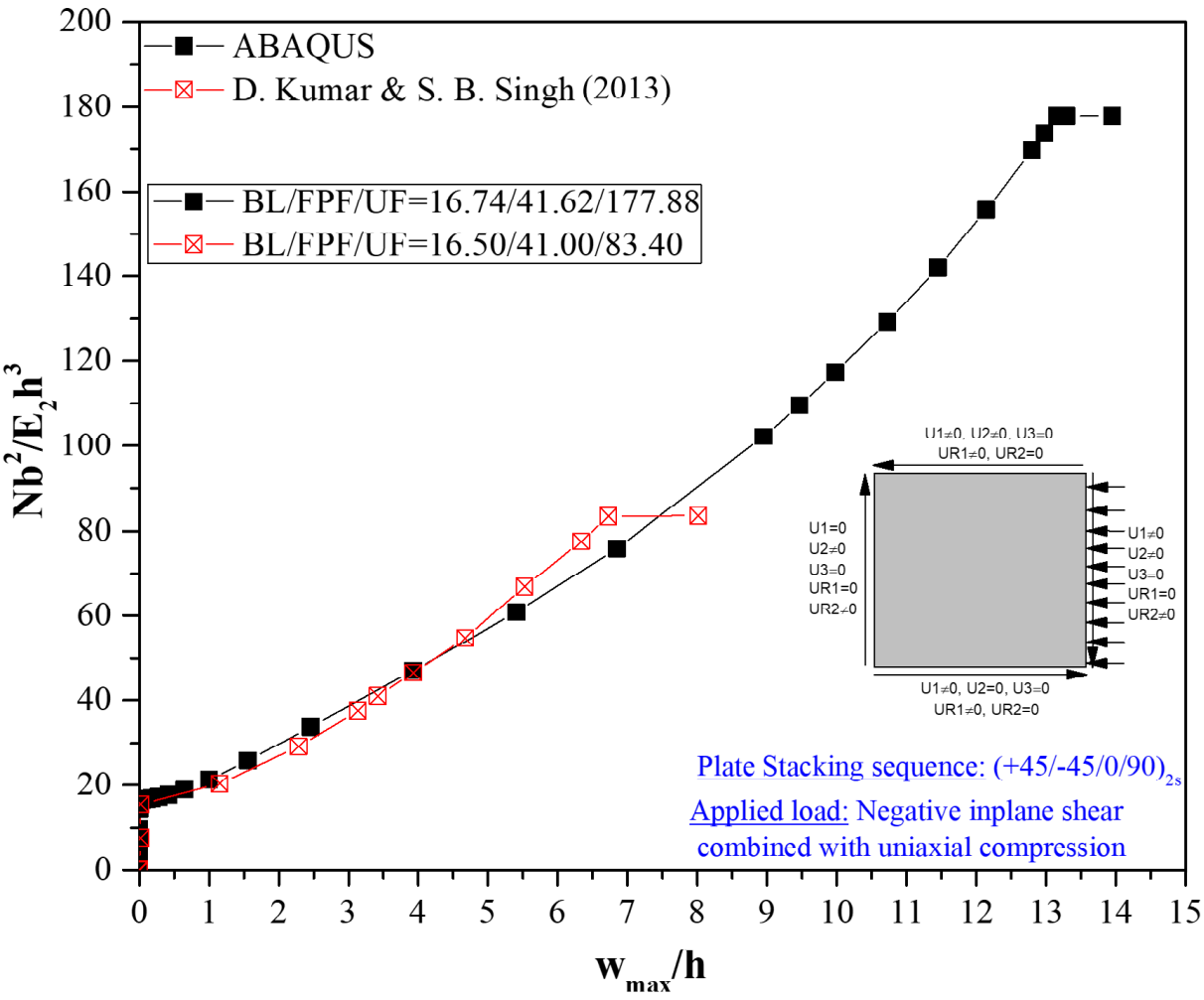

(b)

Fig. 6.2. Validation of published data with ABAQUS of load-deflection responses of the laminate without cutout under: (a) Uni-axial compression combined with positive in-plane shear (b) Uni-axial compression combined with negative in-plane shear

6.2 Verification

The validity of the numerical modelling using ABAQUS has been done by comparing the results with that of published data by Kumar and Singh, 2013 as shown in Fig. 6.2. The same non-linear finite element software (ABAQUS) is used in the present study to determine the buckling and failure loads of composite plates under the combined action of in-plane loads i.e., uniaxial compression and shear. Fig. 6.2(a) and 6.2(b) depicts responses under combined uniaxial compressive load with in-plane positive and negative shear loads, respectively. The critical

buckling, first ply failure and ultimate failure load values are presented in the plot itself. The critical buckling and first ply failure load values are in good agreement with the published load values. This implies the precision and accuracy of the software used in the current study. The ultimate failure loads are considered at a stage when the composite plate is unable to resist any further load i.e., the composite plate is analyzed without any limitations. It may be noted that the ultimate failure loads predicted by Kumar & Singh (2013) and that of the current study using ABAQUS are not in good agreement. This is due to the fact that ultimate load obtained in Kumar & Singh (2013) is based on a computer programming code whereas in ABAQUS numerical study, ultimate failure load is occured at a point where the plate becomes unstable. Geometrically nonlinear problems sometimes involve buckling or collapse behavior. Abaqus offers an automated version of the stabilization approach for the static analysis procedures. Unstable phase of the response can be found by using the modified riks method. The Riks method can be used to solve postbuckling problems both with stable and unstable behaviours. To analyze a postbuckling problem, it must be turned into a problem with continuous response instead of bifurcation. This effect can be accomplished by introducing an initial imperfection into a "perfect" geometry so that there is some response in the buckling mode before the critical load is reached.

This method is used for cases where the loading is proportional i.e., where the load magnitudes are governed by a single scalar parameter (load proportionality factor). This method can provide solutions even in cases of complex and unstable response. In case of problems with material non-linearity, geometric non-linearity prior to buckling or unstable postbuckling response, load-deflection riks analysis must be performed to investigate the problem further. To measure the progress of the solution, arc length quantity is used along the static equilibrium path in load-displacement space. This arc length approach provides solution regardless stable or unstable response. The plate reaches the ultimate load carrying capacity at a specified degree of freedom where it reaches a maximum value of load proportionality factor or a maximum dispacement value. In the current research maximum load magnitude has been considered, further the plate becomes unstable and the drop in load begins. In Figs. 6.2(a) and 6.2(b), 'N' represents the equal value of uniaxial compression and in-plane shear loads i.e., $N_x = N_{xy} = N$.

6.3. Numerical formulation

Finite element analysis-based software (ABAQUS) is used for simulating the postbuckling response of functionally graded hybrid (FH) plates under combined loading condition, i.e., uniaxial compressive load combined with in-plane positive and negative in-plane shear loads, respectively. The model of the functionally graded hybrid laminated plate associated with boundary conditions is shown in Fig. 6.2 as a quick reference. Linear and non-linear buckling and postbuckling numerical analysis of the square symmetric plate with the influence of imperfections are presented. Eigen value linear buckling analysis approach has been used to determine critical buckling load in the first step. Prior to buckling, a very little deformation occurs depending on the magnitude of imperfection.

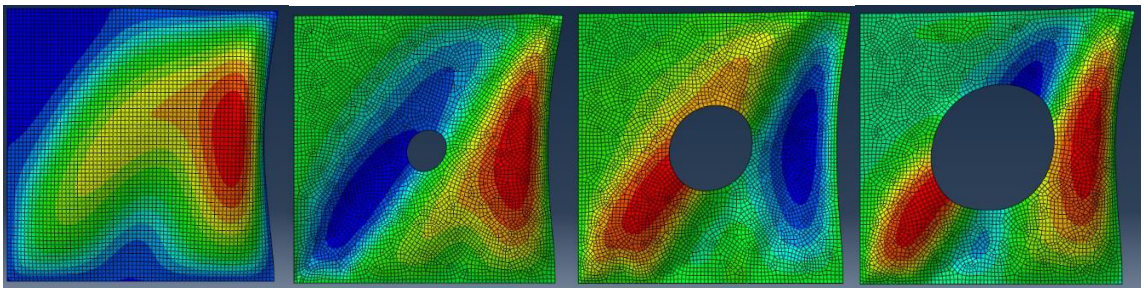

(a) (b) (c) (d)

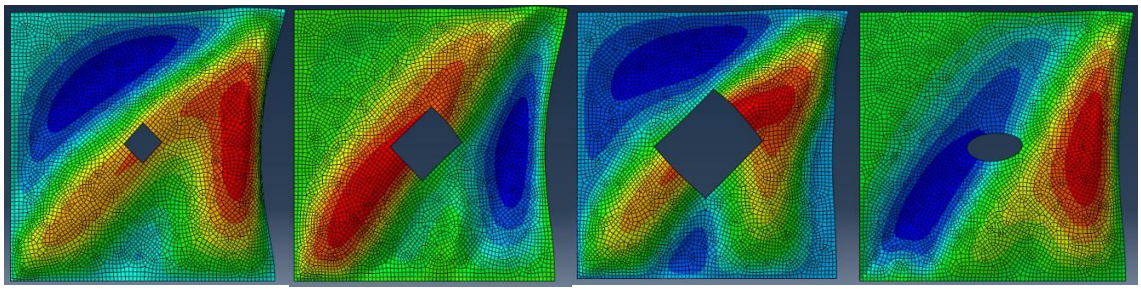

(e) (f) (g) (h)

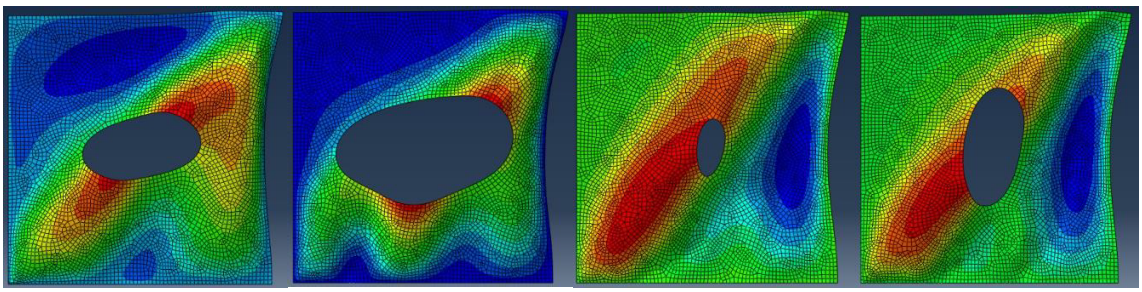

(i) (j) (k) (l)

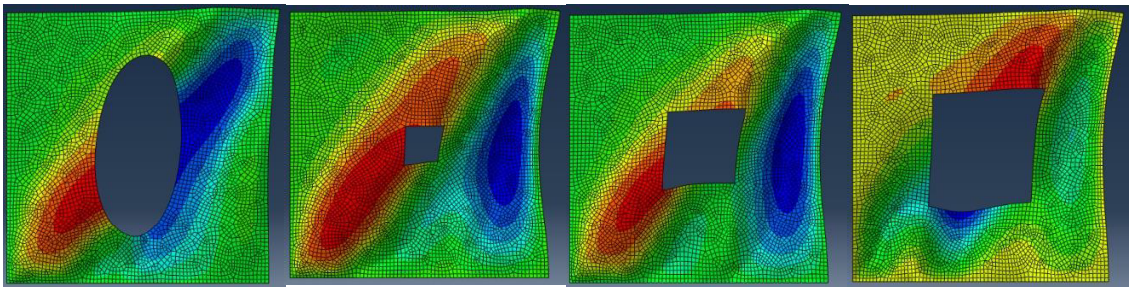

(m) (n) (o) (p)

Fig. 6.3. Failure modes of FH plates with and without cutouts subjected to combined compression and positive in-plane shear loads: (a) FH_NC (b) FH_C1 (c) FH_C2 (d) FH_C3 (e) FH_D1 (f) FH_D2 (g) FH_D3 (h) FH_EH1 (i) FH_EH2 (j) FH_EH3 (k) FH_EV1 (l) FH_EV2 (m) FH_EV3 (n) FH_S1 (o) FH_S2 (p) FH_S3

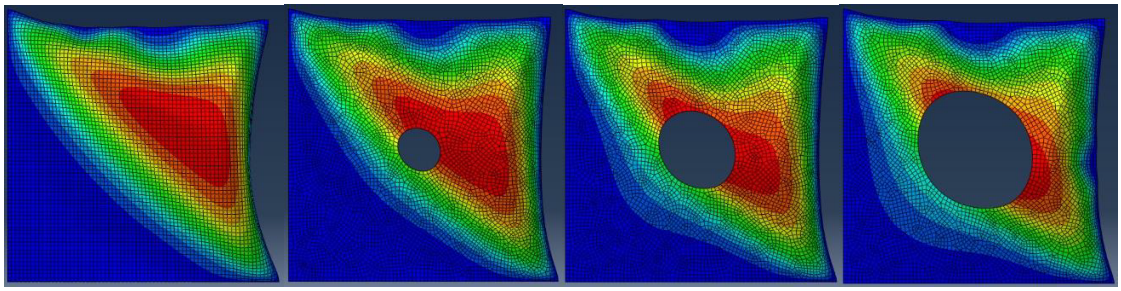

(a) (b) (c) (d)

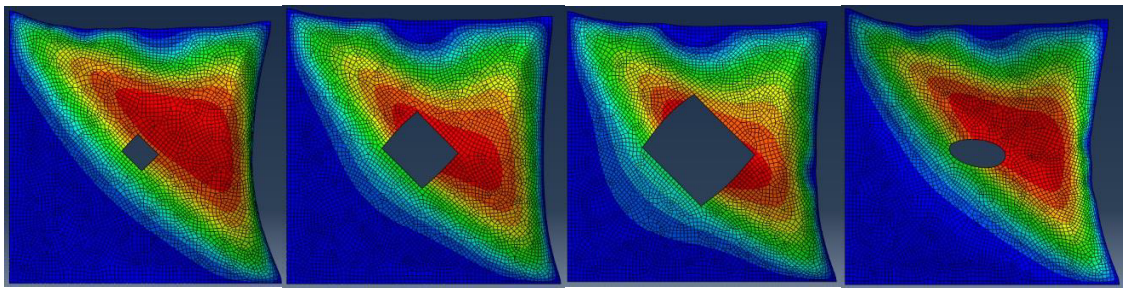

(e) (f) (g) (h)

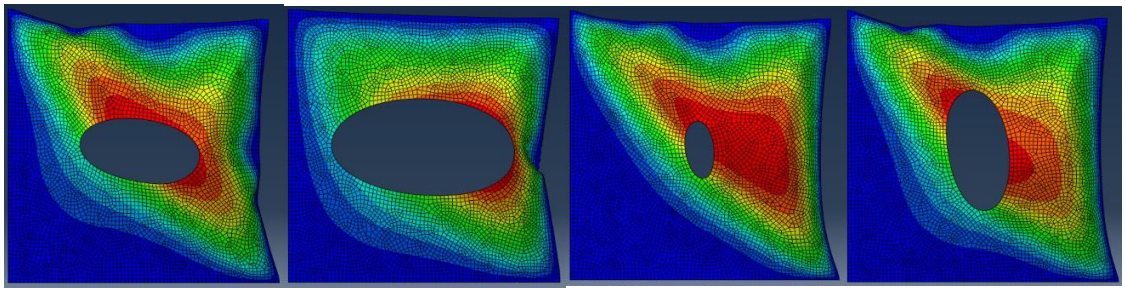

(i) (j) (k) (l)

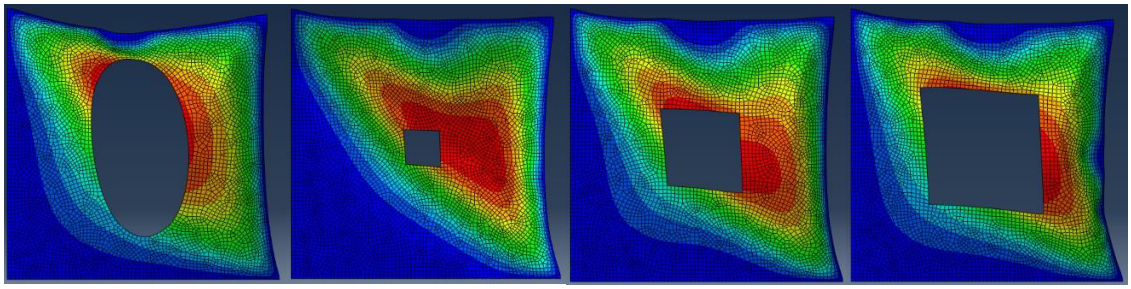

(m) (n) (o) (p)

Fig. 6.4. Failure modes of FH plates with and without cutouts subjected to combined compression and negative in-plane shear loads: (a) FH_NC (b) FH_C1 (c) FH_C2 (d) FH_C3 (e) FH_D1 (f) FH_D2 (g) FH_D3 (h) FH_EH1 (i) FH_EH2 (j) FH_EH3 (k) FH_EV1 (l) FH_EV2 (m) FH_EV3 (n) FH_S1 (o) FH_S2 (p) FH_S3

After the linear buckling analysis, non-linear postbuckling analysis has been performed using static-riks method in which load is increased using a load proportionality factor (LPF) and the structure is configured using an arc length method which allows the procedure to follow the direction of load. This implies that a static-riks step cannot end after a certain pre-prescribed load. Therefore, the procedure ends after reaching a maximum LPF. The behavior of the material is elasto-plastic during nonlinear analysis. To obtain more realistic information of postbuckling response, imperfections are considered. Type of imperfections considered in this study is geometric imperfections. Imperfections highly influence the stability behavior of the plates under the applied load. Shell edge uniaxial compressive load on right most edge and in-plane shear loads are applied on all the four edges of the plate which are simply supported on all the edges. Plate is modelled with four-noded linear shell elements (S4R) with reduced integration in modeling the structure in the current analysis. Finer mesh is used in the current study for accuracy. Meshing was done to the plate with an approximate element size of 0.004m. Mode-I buckling has been considered since the critical buckling occurs in this mode. The failure modes of typical FH plates under combined compression and in-plane positive and negative in-plane shear loads are shown in Fig. 6.3 and Fig. 6.4, respectively. Tsai-Hill failure criterion has been incorporated in the step module of non-linear buckling analysis for determining first failure load which corresponds to first failure of the ply in the plate after the loading is applied. Ultimate failure load is marked at a point where the plate is unable to take any further load. The details of the notations or specimen ID's used in the current study have been presented in Table 6.1.

Table 6.1. Nomenclature of the notations/specimen ID's

Plate ID	Details
FH_NC	Functionally graded hybrid composite plate without cutout
FH_C1	Functionally graded hybrid composite plate with circular shaped cutout of small size*
FH_C2	Functionally graded hybrid composite plate with circular shaped cutout of medium size*
FH_C3	Functionally graded hybrid composite plate with circular shaped cutout of big size*
FH_D1	Functionally graded hybrid composite plate with diamond shaped cutout of small size
FH_D2	Functionally graded hybrid composite plate with diamond shaped cutout of medium size
FH_D3	Functionally graded hybrid composite plate with diamond shaped cutout of big size
FH_EH1	Functionally graded hybrid composite plate with elliptical shaped cutout aligned horizontally of small size
FH_EH2	Functionally graded hybrid composite plate with elliptical shaped cutout aligned horizontally of medium size
FH_EH3	Functionally graded hybrid composite plate with elliptical shaped cutout aligned horizontally of big size
FH_EV1	Functionally graded hybrid composite plate with elliptical shaped cutout aligned vertically of small size
FH_EV2	Functionally graded hybrid composite plate with elliptical shaped cutout aligned vertically of medium size
FH_EV3	Functionally graded hybrid composite plate with elliptical shaped cutout aligned vertically of big size
FH_S1	Functionally graded hybrid composite plate with square shaped cutout of small size
FH_S2	Functionally graded hybrid composite plate with square shaped cutout of medium size
FH_S3	Functionally graded hybrid composite plate with square shaped cutout of big size

*Definition of small, medium, and big size cutout is given in Table 6.2

6.4. Results and discussion

The critical buckling, first ply failure and ultimate failure loads are evaluated for functionally graded hybrid composite plates under uniaxial compression, in-plane shear (positive and negative) and combined compression and in-plane shear loads. In the following sections, results based on finite element analysis using ABAQUS are discussed with regard to effect of stacking sequence, cutout shapes and sizes, and finally the load-interaction curves. The description of cutout shapes and sizes used are presented in Table 6.2 in detail. Typical failure modes are shown in Figs. 6.3

and 6.4. It may be noted that these failure modes are similar for all stacking sequence considered in the study.

Table 6.2. Description of cutout shapes and their sizes

Cutout shape	Ratio♥	Cutout size		
		Small	Medium	Big
Circular (C)	d/b	0.158	0.316	0.474
Diamond (D)	s/b	0.140	0.280	0.420
Ellipse-	e/b	0.224	0.447	0.670
Horizontal (EH)	f/b	0.112	0.223	0.335
Ellipse-Vertical	e/b	0.112	0.223	0.335
(EV)	f/b	0.224	0.447	0.670
Square (S)	s/b	0.140	0.280	0.420

♥These ratios refer to cutouts in Figs. 6.3 and 6.4

Here, 'd' is diameter of the cutout, 'b' is width of the plate, 's' is side of the cutout, 'e' is major axis of the cutout, 'f' is minor axis of the cutout

6.4.1. Effect of stacking sequence

6.4.1.1. $(0/90)_{4s}$ stacking sequence

Among all the FH plates analyzed under different loading conditions, plates subjected to negative in-plane shear has the highest critical buckling load while the lowest critical buckling load can be observed in FH plates subjected to uniaxial compressive load combined with negative in-plane shear as shown in Fig. 6.5(a). Buckling loads of FH plates under positive shear has nearly same value as that for negative shear loaded plates. From Fig. 6.5(a), it is apparent that the difference in the values of buckling loads under positive and negative shear loads combined with uniaxial compression is insignificant. Composite plates without cutouts (NC) however achieves maximum buckling load as expected.

In both the combined loading conditions, i.e., uniaxial compression combined with positive and negative in-plane shear loads, FH plates with small sized cutout have maximum critical buckling load value amongst plates with different sized cutouts. Amidst all the cutouts, FH plates with diamond shaped cutout has higher critical buckling load value. Similar response can be observed in case of first ply failure loads of FH plates as shown in Fig. 6.5(b). As shown in Fig. 6.5(c), ultimate failure loads under combined load case occur in case of positive shear load combined with uniaxial compression.

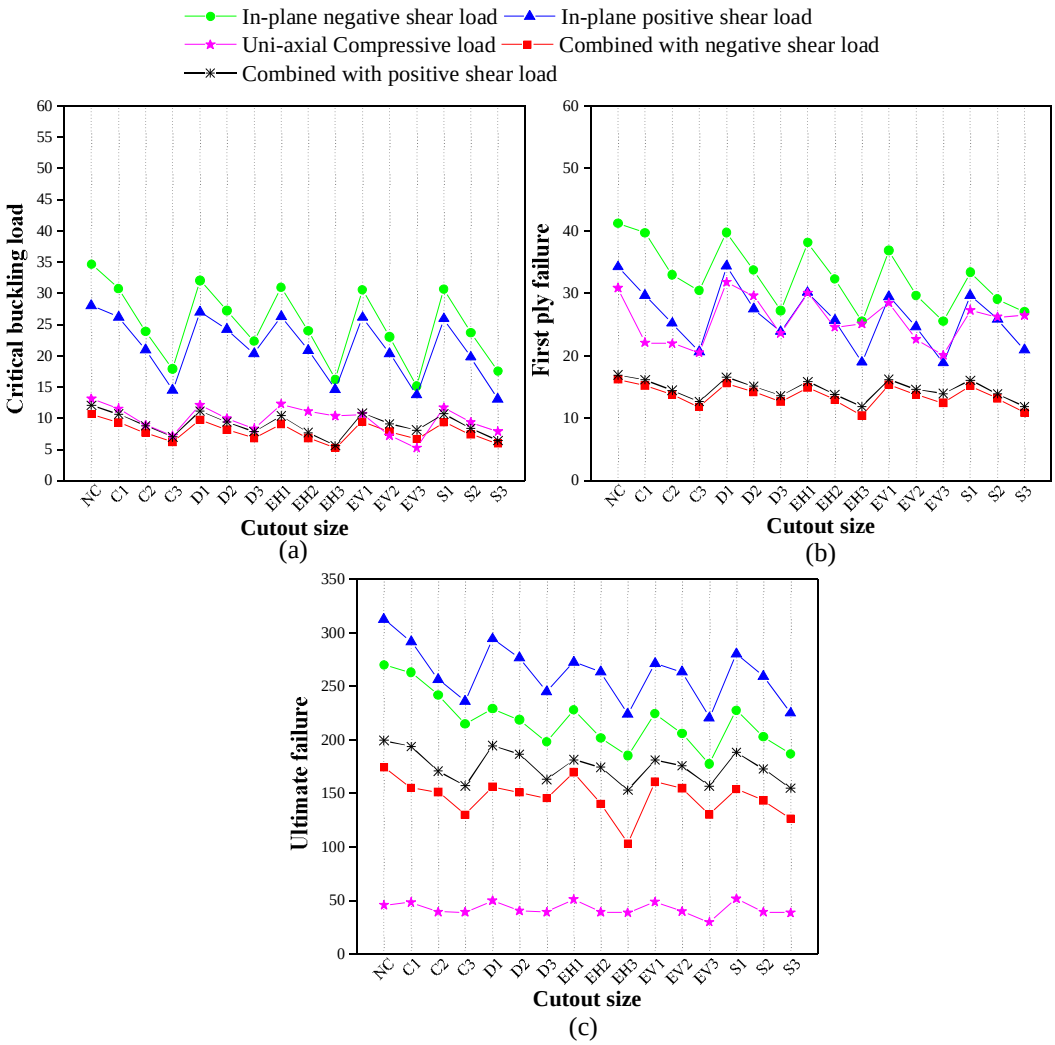

Fig. 6.5. Comparison of (a) Critical buckling load, (b) First ply failure load, and (c) Ultimate failure comparison for FH plates with $(0/90)_{4s}$ stacking sequence under independent action of in-plane shear loads, uniaxial compressive loads, and combined uniaxial compression and in-plane shear loads

However, the highest ultimate failure load is obtained in the case of positive shear while the lowest occurs under uniaxial compression. This may be due to redistribution of stresses after first ply failure. The numerical representation of all the buckling and failure load values of plates with $(0/90)_{4s}$ stacking sequence are depicted in Table 6.3.

Table 6.3. Buckling and first ply failure loads of FH plates with stacking sequence $(0/90)_{4s}$

Specimen ID	Uniaxial Compressive load (A) BL(FPF)♣	Positive In-plane Shear load (B) BL(FPF)♣	Negative In-plane shear load (C) BL(FPF)♣	Combined loading (A+B) BL(FPF)♣	Combined loading (A+C) BL(FPF)♣
FH_NC*	13.08(30.81)♣	28.04(34.23)	34.61(41.18)	12.07(16.91)	10.65(16.20)
FH_C1	11.54(22.09)	26.17(29.64)	30.7139.68)	10.64(16.14)	9.27(15.24)
FH_C2	8.92(21.95)	20.93(25.21)	23.87(32.95)	8.80(14.47)	7.66(13.76)
FH_C3	7.21(20.51)	14.53(20.67)	17.89(30.44)	6.99(12.68)	6.21(11.77)
FH_D1	12.07(31.78)	27.02(34.34)	32.04(39.73)	11.13(16.55)	9.72(15.57)
FH_D2	9.93(29.59)	24.25(27.50)	27.18(33.70)	9.38(15.09)	8.13(14.22)
FH_D3	8.33(23.61)	20.35(23.87)	22.32(27.24)	7.82(13.63)	6.82(12.65)
FH_EH1	12.28(30.07)	26.28(30.12)	30.92(38.13)	10.40(15.89)	9.08(14.91)
FH_EH2	11.11(24.57)	20.88(25.63)	23.98(32.26)	7.71(13.84)	6.83(12.90)
FH_EH3	10.31(25.10)	14.58(18.96)	16.18(25.53)	5.60(11.86)	5.24(10.41)
FH_EV1	10.63(28.43)	26.12(29.48)	30.55(36.85)	10.85(16.20)	9.44(15.36)
FH_EV2	7.21(22.63)	20.35(24.67)	23.02(29.64)	9.10(14.64)	7.85(13.72)
FH_EV3	5.23(20.08)	13.73(18.85)	15.11(25.53)	8.11(13.96)	6.65(12.43)
FH_S1	11.70(27.31)	25.90(29.69)	30.65(33.38)	10.69(16.06)	9.34(15.20)
FH_S2	9.35(26.22)	19.76(25.85)	23.71(29.05)	8.38(13.90)	7.41(13.19)
FH_S3	7.85(25.44)	13.03(20.99)	17.52(27.02)	6.43(11.82)	5.94(10.85)

Note: All the values are non-dimensional (i.e., Nb^2/E_2h^3) (Here, N can be taken as N_x and N_{xy})
where, N_x is Uni-axial compressive load, N_{xy} is In-plane shear load; b is width of the plate; E_2 is transverse modulus; h is thickness of the plate
♣Buckling load (First ply Failure load)

6.4.1.2. $(+45/-45)_{4s}$ stacking sequence

In the plates with $(+45/-45)_{4s}$ stacking sequence, FH plates subjected to combined compression with negative in-plane shear loads have higher critical buckling and first ply failure loads than plates under combined compression load with positive in-plane shear as shown in Figs. 6.6(a) and 6.6(b). It is also observed that plates with small cutout sizes have maximum critical buckling and first ply failure loads regardless the cutout shape. Alike FH plates with $(0/90)_{4s}$ stacking sequence, diamond shaped cutout plate is efficient in terms of critical buckling and first ply failure of laminates. Highest ultimate failure loads of FH plates occurred in plates with elliptical shaped cutout aligned vertically as shown in Fig. 6.6(c). The numerical representation of all the buckling and failure load values of plates with fiber aligned in (+45/-45) direction are presented in Table 6.4.

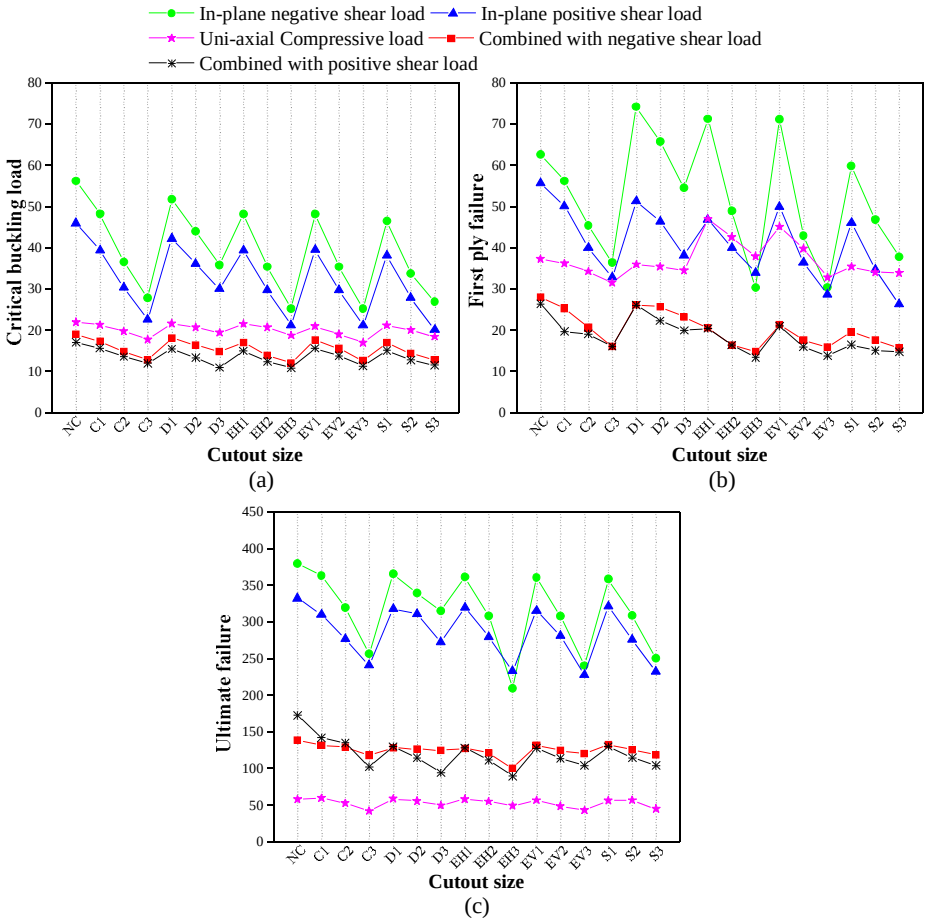

Fig. 6.6. Comparison of (a) Critical buckling load, (b) First ply failure load, and (c) Ultimate failure comparison for FH plates with $(+45/-45)_{4s}$ stacking sequence under independent action of in-plane shear loads, uniaxial compressive loads, and combined uniaxial compression and in-plane shear loads

Table 6.4. Buckling and first ply failure loads of FH plates with stacking sequence $(+45/-45)_{4s}$

Specimen ID	Uniaxial Compressive load (A) BL(FPF)♣	Positive In-plane Shear load (B) BL(FPF)♣	Negative In-plane shear load (C) BL(FPF)♣	Combined loading (A+B) BL(FPF)♣	Combined loading (A+C) BL(FPF)♣
FH_NC	22.00(37.28)♣	45.98(55.65)	56.18(62.59)	17.08(26.42)	19.06(28.03)
FH_C1	21.31(36.21)	39.41(50.09)	48.28(56.18)	15.69(19.74)	17.30(25.31)
FH_C2	19.76(34.29)	30.39(40.00)	36.58(45.39)	13.61(19.14)	14.81(20.68)
FH_C3	17.78(31.56)	22.64(32.84)	27.82(36.48)	12.02(16.08)	12.80(16.10)
FH_D1	21.63(35.99)	42.24(51.32)	51.75(74.23)	15.49(26.07)	18.11(26.23)
FH_D2	20.72(35.41)	36.16(46.41)	43.95(65.79)	13.37(22.31)	16.40(25.74)
FH_D3	19.39(34.49)	30.07(38.24)	35.83(54.53)	10.97(20.00)	14.82(23.28)
FH_EH1	21.58(47.01)	39.41(46.89)	48.17(71.24)	15.03(20.43)	17.00(20.51)

FH_EH2	20.72(42.62)	29.69(40.05)	35.41(48.92)	12.44(16.39)	13.95(16.40)
FH_EH3	18.80(37.97)	21.26(34.02)	25.26(30.39)	10.90(13.47)	12.11(14.80)
FH_EV1	20.99(45.14)	39.47(49.88)	48.17(71.14)	15.63(21.03)	17.64(21.36)
FH_EV2	19.01(39.84)	29.69(36.48)	35.41(42.99)	13.84(16.02)	15.56(17.68)
FH_EV3	16.98(32.83)	21.26(28.68)	25.26(30.44)	11.34(13.85)	12.66(15.91)
FH_S1	21.26(35.41)	38.13(46.04)	46.52(59.81)	15.12(16.51)	16.97(19.60)
FH_S2	20.03(34.11)	27.98(34.71)	33.81(46.89)	12.83(15.11)	14.37(17.69)
FH_S3	18.48(33.91)	20.13(26.33)	26.92(37.81)	12.02(14.78)	12.80(15.75)

Note: All the values are non-dimensional (i.e., Nb^2/E_2h^3) (Here, N can be taken as N_x and N_{xy})

♣Buckling load (First ply Failure load)

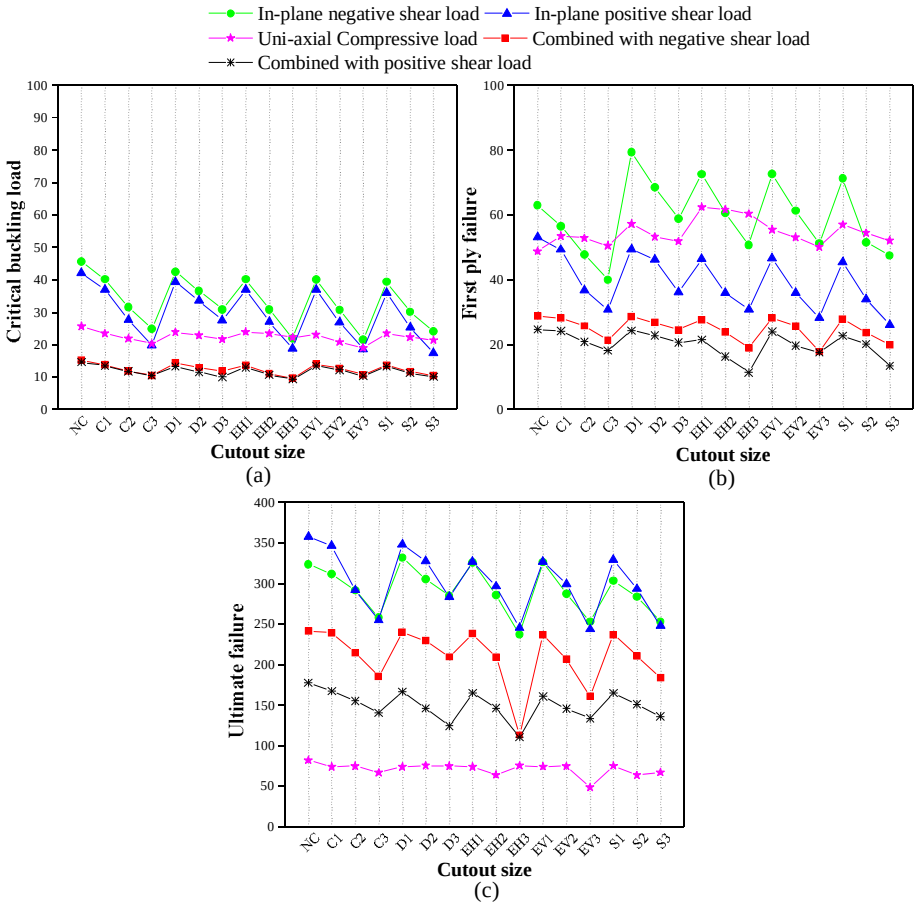

Fig. 6.7. Comparison of (a) Critical buckling load, (b) First ply failure load, and (c) Ultimate failure load comparison for FH plates with $(+45/-45/0/90)_{2s}$ stacking sequence under independent action of in-plane shear loads, uniaxial compressive loads, and combined uniaxial compression and in-plane shear loads

6.4.1.3. $(+45/-45/0/90)_{2s}$ stacking sequence

In functionally graded hybrid composite plates with quasi-isotropic stacking sequence, the trend is similar to the plates aligned in $(+45/-45)_{4s}$ fiber stacking sequence as shown in Fig. 6.7. The compressive loads combined with negative in-plane shear outperformed in comparison with the combined compressive and positive in-plane shear loads in terms of buckling, first ply failure and ultimate failure loads. The numerical representation of all the buckling and failure load values of plates with fiber aligned in (+45/-45/0/90) direction are depicted in Table 6.5. It is clear from Tables 6.3 to 6.5 that, this laminate has better strength than other laminates.

Table 6.5. Buckling and first ply failure loads of FH plates with stacking sequence $(+45/-45/0/90)_{2s}$

Specimen ID	Uniaxial Compressive load (A) BL(FPF)♣	Positive In-plane Shear load (B) BL(FPF)♣	Negative In-plane shear load (C) BL(FPF)♣	Combined loading (A+B) BL(FPF)♣	Combined loading (A+C) BL(FPF)♣
FH_NC	25.74(48.87)♣	42.19(53.24)	45.66(63.02)	15.73(25.51)	16.17(28.95)
FH_C1	23.50(53.57)	37.06(49.35)	40.21(56.61)	13.58(24.26)	13.82(28.25)
FH_C2	21.95(52.92)	27.77(36.85)	31.62(47.85)	11.83(20.93)	11.87(25.85)
FH_C3	20.35(50.61)	19.76(30.87)	24.99(40.05)	10.54(18.26)	10.59(21.47)
FH_D1	23.87(57.30)	39.36(49.51)	42.51(79.36)	14.87(27.77)	15.40(28.63)
FH_D2	22.91(53.35)	33.59(46.25)	36.64(68.57)	11.60(22.83)	13.00(26.86)
FH_D3	21.74(51.91)	27.61(36.26)	30.92(58.85)	10.11(20.70)	11.87(24.57)
FH_EH1	23.98(62.47)	37.01(46.57)	40.21(72.63)	13.04(21.59)	13.59(27.77)
FH_EH2	23.50(61.68)	27.13(36.05)	30.92(60.67)	10.76(16.36)	11.14(24.06)
FH_EH3	22.32(60.40)	18.80(30.81)	21.95(50.73)	9.36(11.51)	9.68(19.18)
FH_EV1	23.07(55.54)	37.01(46.62)	40.16(72.68)	13.58(24.06)	14.12(28.30)
FH_EV2	20.83(53.18)	27.02(35.99)	30.76(61.36)	12.25(19.70)	12.71(25.74)
FH_EV3	19.07(50.22)	18.64(28.30)	21.63(51.32)	10.40(17.66)	10.81(17.94)
FH_S1	23.50(57.04)	35.99(45.50)	39.41(71.30)	13.25(22.80)	13.70(27.88)
FH_S2	22.38(54.52)	25.31(34.02)	30.17(51.59)	11.33(20.24)	11.75(23.71)
FH_S3	21.47(52.18)	17.46(26.22)	24.14(47.58)	10.15(13.55)	10.50(20.08)

Note: All the values are non-dimensional (i.e., Nb^2/E_2h^3) (Here, N can be taken as N_x and N_{xy})
♣Buckling load (First ply Failure load)

6.4.2. Effect of cutout shape and size

In this section, the effect of cutout shape and size on postbuckling response of FH plate with $(0/90)_{4s}$, $(+45/-45)_{4s}$ and $(+45/-45/0/90)_{2s}$ stacking sequences under combined in-plane loading conditions is discussed. The load-deflection response of functionally graded hybrid composite plate with various shaped and sized cutouts with fiber aligned in (0/90), (+45/-45), and (+45/-

45/0/90) directions are shown in Figs. 6.8, 6.9, and 6.10, respectively. The ratio of uniaxial compressive load to the in-plane shear load (positive and negative) is taken to be unity in Figs. 6.8, 6.9, and 6.10 i.e., $N_x/N_{xy} = 1$. In figures, 'N' represents the equal value of uniaxial compression and in-plane shear loads i.e., $N_x = N_{xy} = N$.

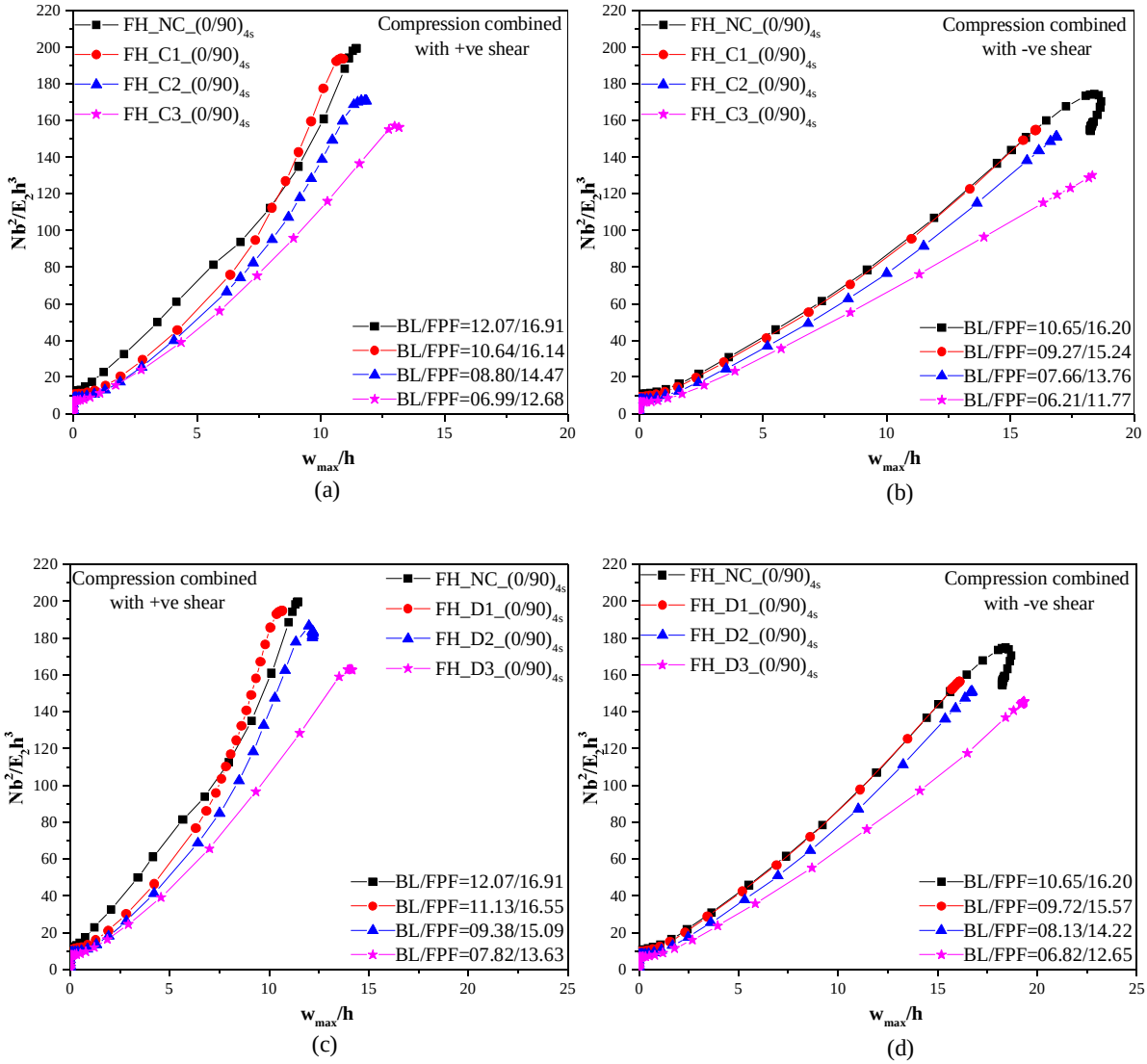

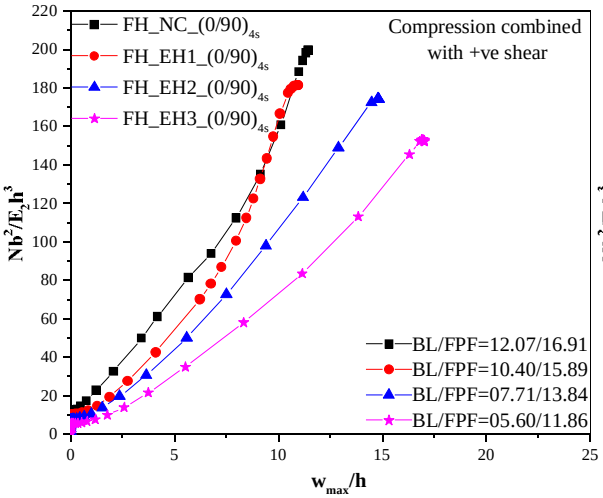
FH_NC_(0/90)4s
FH_EH1_(0/90)4s
FH_EH2_(0/90)4s
FH_EH3_(0/90)4s
Compression combined with +ve shear
BL/FPF=12.07/16.91
BL/FPF=10.40/15.89
BL/FPF=07.71/13.84
BL/FPF=05.60/11.86
Nb²/E2h³
wmax/h

(e)

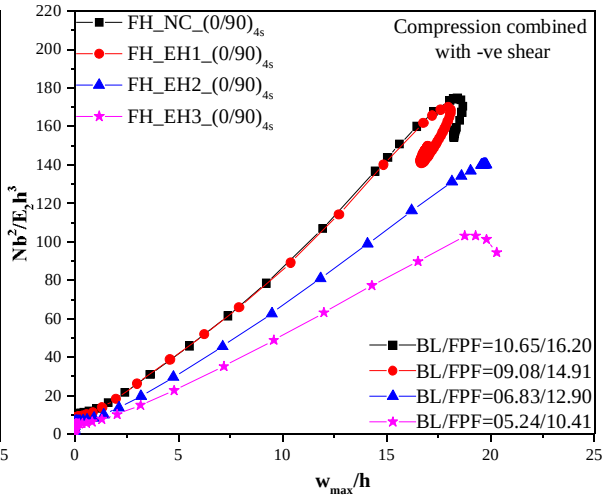
FH_NC_(0/90)4s
FH_EH1_(0/90)4s
FH_EH2_(0/90)4s
FH_EH3_(0/90)4s
Compression combined with -ve shear
BL/FPF=10.65/16.20
BL/FPF=09.08/14.91
BL/FPF=06.83/12.90
BL/FPF=05.24/10.41
Nb²/E2h³
wmax/h

(f)

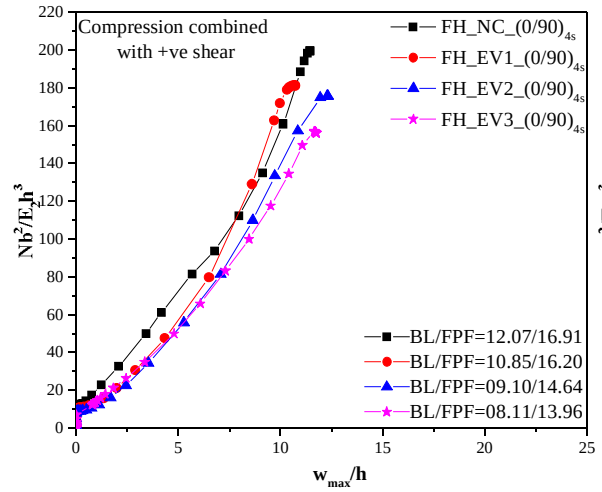
Compression combined with +ve shear
FH_NC_(0/90)4s
FH_EV1_(0/90)4s
FH_EV2_(0/90)4s
FH_EV3_(0/90)4s
BL/FPF=12.07/16.91
BL/FPF=10.85/16.20
BL/FPF=09.10/14.64
BL/FPF=08.11/13.96
Nb²/E2h³
wmax/h

(g)

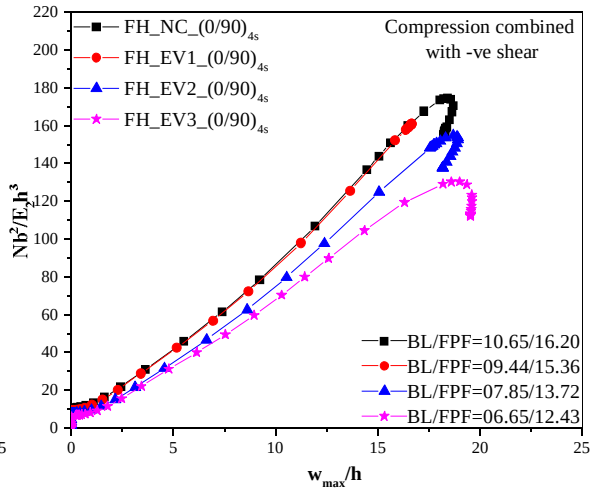
FH_NC_(0/90)4s
FH_EV1_(0/90)4s
FH_EV2_(0/90)4s
FH_EV3_(0/90)4s
Compression combined with -ve shear
BL/FPF=10.65/16.20
BL/FPF=09.44/15.36
BL/FPF=07.85/13.72
BL/FPF=06.65/12.43
Nb²/E2h³
wmax/h

(h)

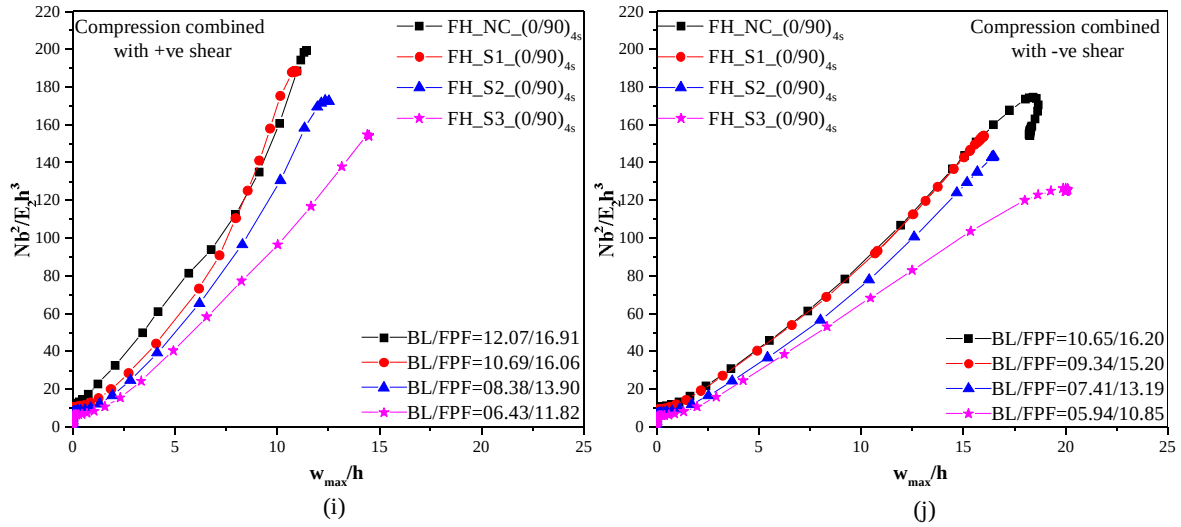

Fig. 6.8. Non-dimensional load-deflection responses of functionally graded hybrid plates aligned in (0/90) fiber direction with different sized cutouts: (a) Circular shaped cutouts under compressive load combined with +ve shear (b) Circular shaped cutouts under compressive load combined with -ve shear (c) Diamond shaped cutouts under compressive load combined with +ve shear (d) Diamond shaped cutouts under compressive load combined with -ve shear (e) Ellipse horizontal shaped cutouts under compressive load combined with +ve shear (f) Ellipse horizontal shaped cutouts under compressive load combined with -ve shear (g) Ellipse vertical shaped cutouts under compressive load combined with +ve shear (h) Ellipse vertical shaped cutouts under compressive load combined with -ve shear (i) Square shaped cutouts under compressive load combined with +ve shear (j) Square shaped cutouts under compressive load combined with -ve shear

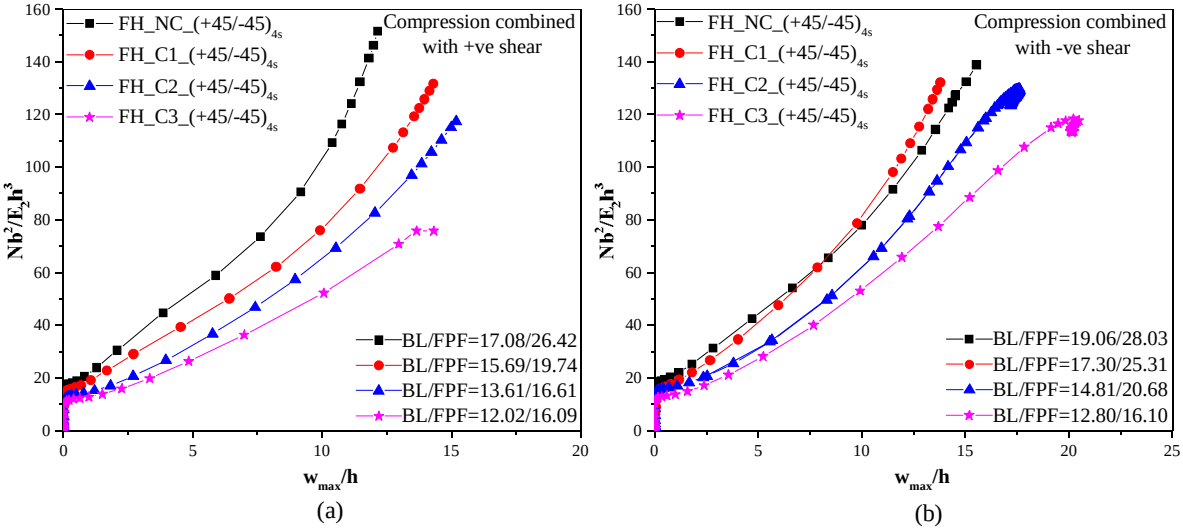

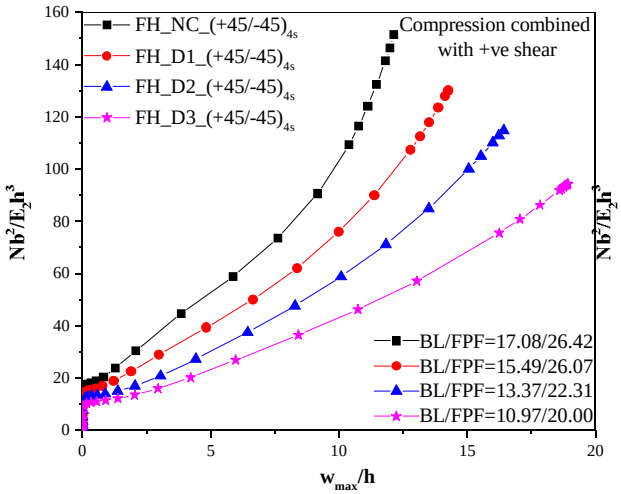
FH_NC_(+45/-45)4s
FH_D1_(+45/-45)4s
FH_D2_(+45/-45)4s
FH_D3_(+45/-45)4s
Compression combined with +ve shear
BL/FPF=17.08/26.42
BL/FPF=15.49/26.07
BL/FPF=13.37/22.31
BL/FPF=10.97/20.00
Nb²/E2h³
wmax/h

(c)

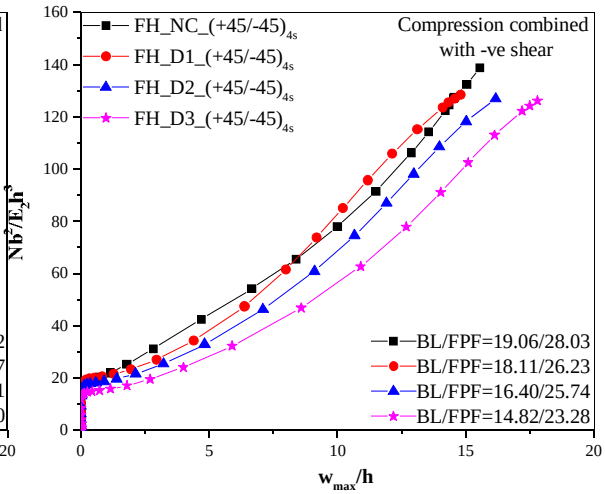
FH_NC_(+45/-45)4s
FH_D1_(+45/-45)4s
FH_D2_(+45/-45)4s
FH_D3_(+45/-45)4s
Compression combined with -ve shear
BL/FPF=19.06/28.03
BL/FPF=18.11/26.23
BL/FPF=16.40/25.74
BL/FPF=14.82/23.28
Nb²/E2h³
wmax/h

(d)

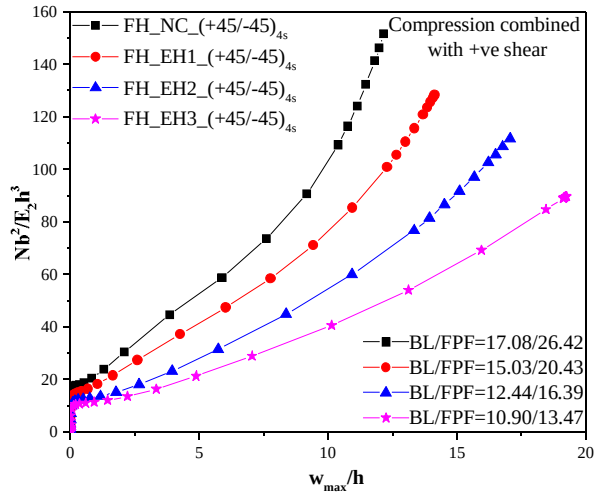
FH_NC_(+45/-45)4s
FH_EH1_(+45/-45)4s
FH_EH2_(+45/-45)4s
FH_EH3_(+45/-45)4s
Compression combined with +ve shear
BL/FPF=17.08/26.42
BL/FPF=15.03/20.43
BL/FPF=12.44/16.39
BL/FPF=10.90/13.47
Nb²/E2h³
wmax/h

(e)

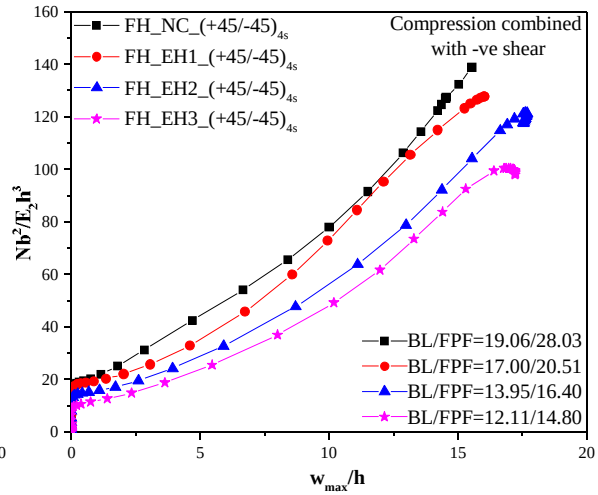
FH_NC_(+45/-45)4s
FH_EH1_(+45/-45)4s
FH_EH2_(+45/-45)4s
FH_EH3_(+45/-45)4s
Compression combined with -ve shear
BL/FPF=19.06/28.03
BL/FPF=17.00/20.51
BL/FPF=13.95/16.40
BL/FPF=12.11/14.80
Nb²/E2h³
wmax/h

(f)

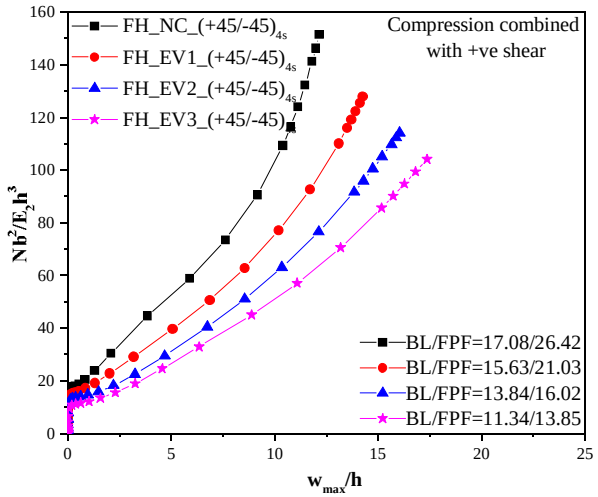
FH_NC_(+45/-45)4s
FH_EV1_(+45/-45)4s
FH_EV2_(+45/-45)4s
FH_EV3_(+45/-45)4s
Compression combined with +ve shear
BL/FPF=17.08/26.42
BL/FPF=15.63/21.03
BL/FPF=13.84/16.02
BL/FPF=11.34/13.85
Nb²/E2h³
wmax/h

(g)

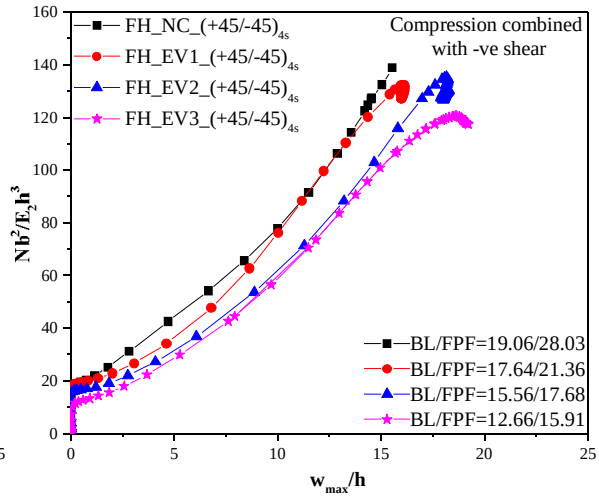
FH_NC_(+45/-45)4s
FH_EV1_(+45/-45)4s
FH_EV2_(+45/-45)4s
FH_EV3_(+45/-45)4s
Compression combined with -ve shear
BL/FPF=19.06/28.03
BL/FPF=17.64/21.36
BL/FPF=15.56/17.68
BL/FPF=12.66/15.91
Nb²/E2h³
wmax/h

(h)

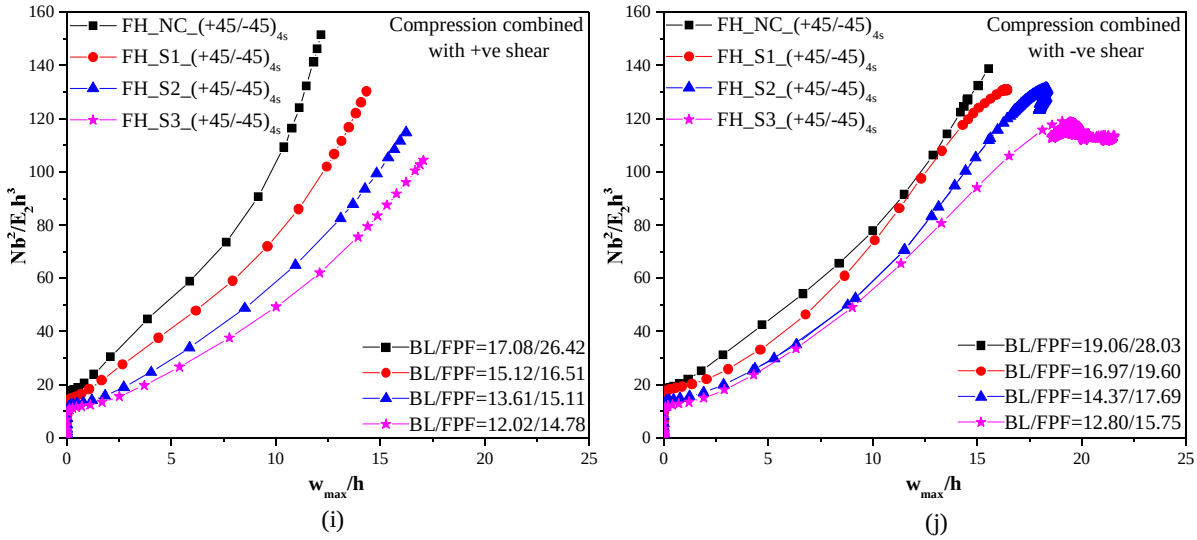

Fig. 6.9. Non-dimensional load-deflection responses of functionally graded hybrid plates aligned in (+45/-45) fiber direction with different sized cutouts: (a) Circular shaped cutouts under compressive load combined with +ve shear (b) Circular shaped cutouts under compressive load combined with -ve shear (c) Diamond shaped cutouts under compressive load combined with +ve shear (d) Diamond shaped cutouts under compressive load combined with -ve shear (e) Ellipse horizontal shaped cutouts under compressive load combined with +ve shear (f) Ellipse horizontal shaped cutouts under compressive load combined with -ve shear (g) Ellipse vertical shaped cutouts under compressive load combined with +ve shear (h) Ellipse vertical shaped cutouts under compressive load combined with -ve shear (i) Square shaped cutouts under compressive load combined with +ve shear (j) Square shaped cutouts under compressive load combined with -ve shear

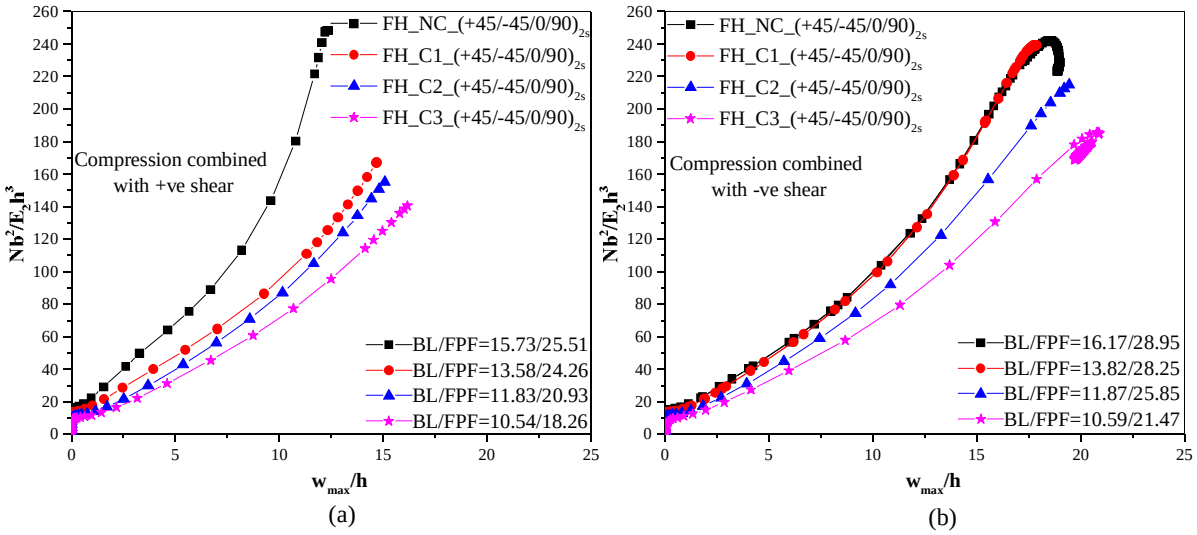

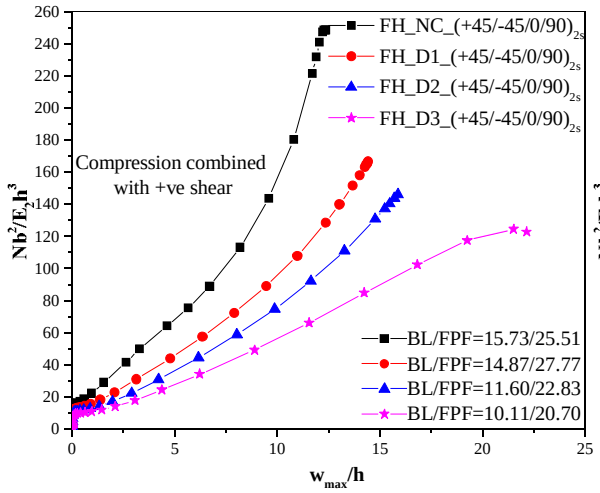
FH_NC_(+45/-45/0/90)2s
FH_D1_(+45/-45/0/90)2s
FH_D2_(+45/-45/0/90)2s
FH_D3_(+45/-45/0/90)2s
Compression combined with +ve shear
BL/FPF=15.73/25.51
BL/FPF=14.87/27.77
BL/FPF=11.60/22.83
BL/FPF=10.11/20.70
Nb²/E2h³
wmax/h

(c)

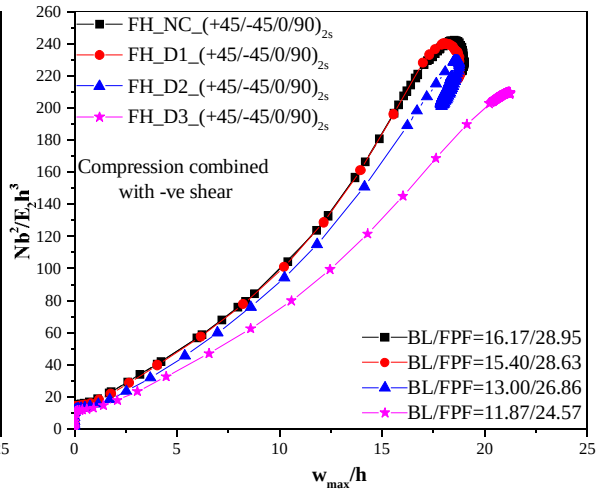
FH_NC_(+45/-45/0/90)2s
FH_D1_(+45/-45/0/90)2s
FH_D2_(+45/-45/0/90)2s
FH_D3_(+45/-45/0/90)2s
Compression combined with -ve shear
BL/FPF=16.17/28.95
BL/FPF=15.40/28.63
BL/FPF=13.00/26.86
BL/FPF=11.87/24.57
Nb²/E2h³
wmax/h

(d)

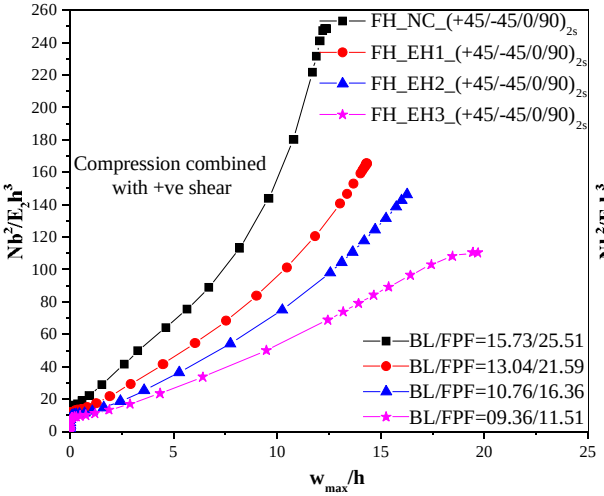
FH_NC_(+45/-45/0/90)2s
FH_EH1_(+45/-45/0/90)2s
FH_EH2_(+45/-45/0/90)2s
FH_EH3_(+45/-45/0/90)2s
Compression combined with +ve shear
BL/FPF=15.73/25.51
BL/FPF=13.04/21.59
BL/FPF=10.76/16.36
BL/FPF=09.36/11.51
Nb²/E2h³
wmax/h

(e)

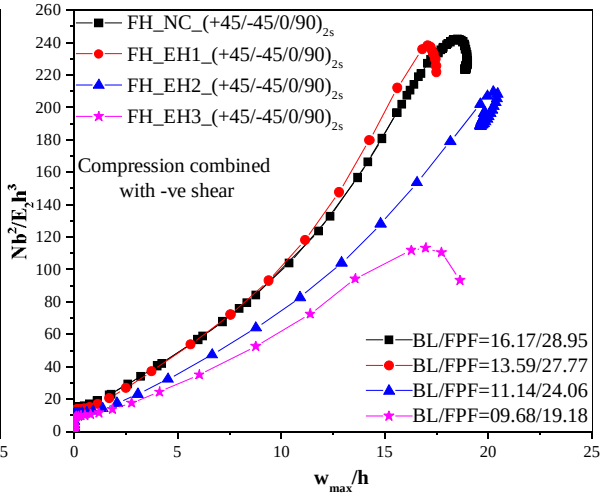
FH_NC_(+45/-45/0/90)2s
FH_EH1_(+45/-45/0/90)2s
FH_EH2_(+45/-45/0/90)2s
FH_EH3_(+45/-45/0/90)2s
Compression combined with -ve shear
BL/FPF=16.17/28.95
BL/FPF=13.59/27.77
BL/FPF=11.14/24.06
BL/FPF=09.68/19.18
Nb²/E2h³
wmax/h

(f)

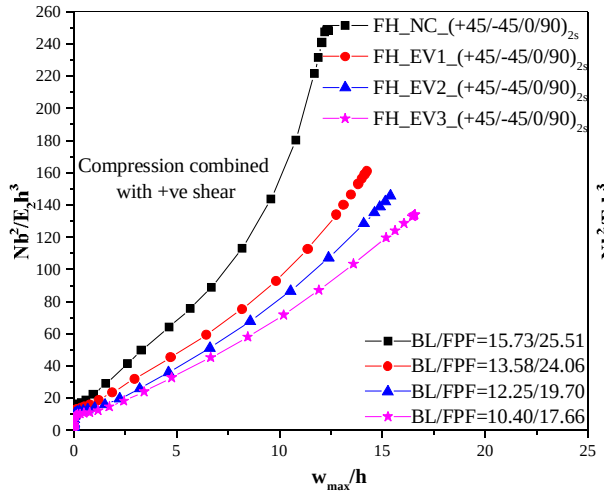
FH_NC_(+45/-45/0/90)2s
FH_EV1_(+45/-45/0/90)2s
FH_EV2_(+45/-45/0/90)2s
FH_EV3_(+45/-45/0/90)2s
Compression combined with +ve shear
BL/FPF=15.73/25.51
BL/FPF=13.58/24.06
BL/FPF=12.25/19.70
BL/FPF=10.40/17.66
Nb²/E2h³
wmax/h

(g)

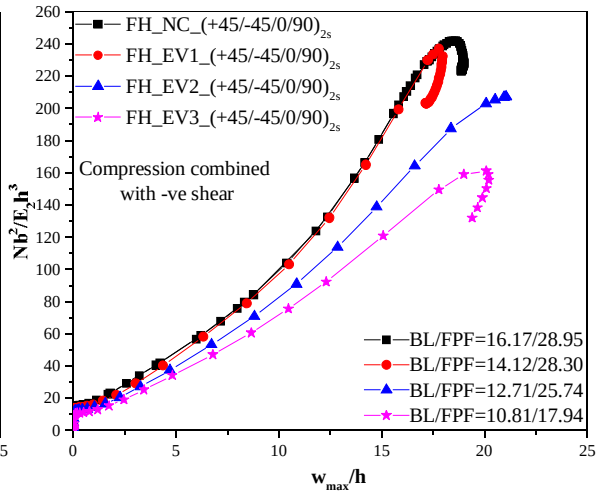
FH_NC_(+45/-45/0/90)2s
FH_EV1_(+45/-45/0/90)2s
FH_EV2_(+45/-45/0/90)2s
FH_EV3_(+45/-45/0/90)2s
Compression combined with -ve shear
BL/FPF=16.17/28.95
BL/FPF=14.12/28.30
BL/FPF=12.71/25.74
BL/FPF=10.81/17.94
Nb²/E2h³
wmax/h

(h)

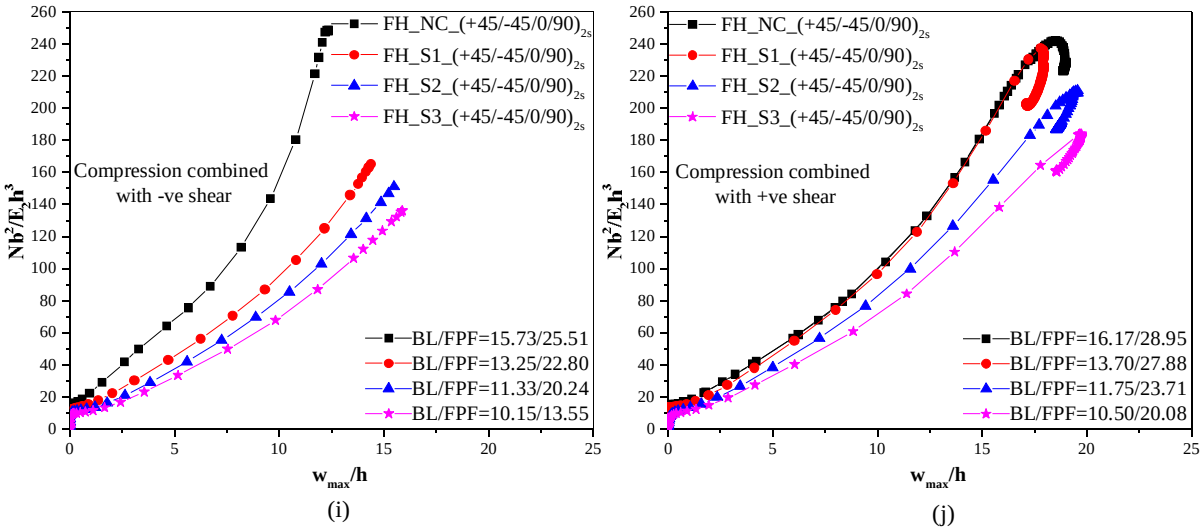

Fig. 6.10. Non-dimensional load-deflection responses of functionally graded hybrid plates aligned in quasi-isotropic (+45/-45/0/90) fiber direction with different sized cutouts: (a) Circular shaped cutouts under compressive load combined with +ve shear (b) Circular shaped cutouts under compressive load combined with -ve shear (c) Diamond shaped cutouts under compressive load combined with +ve shear (d) Diamond shaped cutouts under compressive load combined with -ve shear (e) Ellipse horizontal shaped cutouts under compressive load combined with +ve shear (f) Ellipse horizontal shaped cutouts under compressive load combined with -ve shear (g) Ellipse vertical shaped cutouts under compressive load combined with +ve shear (h) Ellipse vertical shaped cutouts under compressive load combined with -ve shear (i) Square shaped cutouts under compressive load combined with +ve shear (j) Square shaped cutouts under compressive load combined with -ve shear

The initial observation that can be made from Fig. 6.8(a) is that for a specific deflection, the plate FH_C1_$(0/90)_{4s}$ has the maximum postbuckling strength, although the critical buckling and ultimate failure load is higher in FH plate without cutout. So, in plates with cutouts, smaller size cutout has maximum buckling, first ply failure and ultimate failure loads when compared to other sized cutouts. In case of FH plate subjected to combined compression and negative in-plane shear load, FH_NC_$(0/90)_{4s}$ and FH_C1_$(0/90)_{4s}$ has similar postbuckling strength at a particular w_{max}/h value as shown in Fig. 6.8(b). It is also observed that, direction of shear load has a significant effect on ultimate failure loads. The compression loaded plates combined with positive shear load has maximum ultimate load values than loads combined with negative shear in $(0/90)_{4s}$ layup sequence plates. Similar trend is observed in the plates with diamond, elliptical and square shaped cutouts with fiber aligned in (0/90) direction as shown in Figs. 6.8(c to j). The critical buckling load value is observed to be maximum in FH plate with diamond shaped cutout amidst all. This

result indicates that introduction of a small size cutout does not reduce the postbuckling strength of FH plates with $(0/90)_{4s}$ stacking sequence.

In case of FH plates with fiber aligned in $(+45/-45)_{4s}$ directions, plates subjected to combined compression and negative in-plane shear loads are observed to have maximum buckling and first ply failure loads as shown in Fig. 6.9. The load-deflection response curves under combined uniaxial compression and positive in-plane shear for a given deflection, load is higher for smaller size cutout as shown in Figs. 6.9(a, c, e, g, i). All these plates are subjected to combined compression and positive shear. In plates combined with compression and negative in-plane shear loads, from Fig. 6.9(b) it is observed that, after a particular deflection value, postbuckling response of FH_C1_$(+45/-45)_{4s}$ is higher that the plate without cutout i.e., FH_NC_$(+45/-45)_{4s}$. It is observed in case of plate with diamond shaped cutout, but at the ultimate failure point, these plots coincide again as shown in Fig. 6.9(d) because of redistribution of stresses. Load-deflection plots of elliptical and square shaped cutouts show a similar trend, i.e., at a certain value of w_{max}/h, postbuckling strengths of FH_NC_$(+45/-45)_{4s}$ unite with FH_EV1_$(+45/-45)_{4s}$ as shown in Fig. 6.9(h) and nearly approaches the peripheral (or edge) of FH_EH1_$(+45/-45)_{4s}$ and FH_S1_$(+45/-45)_{4s}$ as shown in Figs. 6.9(f) and 6.9(j), respectively. From the strength point of view, FH plate with diamond shaped cutout is recommended for the structural applications while the size of diamond cutout outperformed is smaller size (i.e., 14% as shown in Table 6.2) of the width of the FH composite plate.

In quasi-isotropic $(+45/-45/0/90)_{2s}$ fiber aligned composite plates, the postbuckling strength of plates without cutouts subjected to combined compression and positive in-plane shear loads are observed to be very high compared to the plates with cutouts as shown in Figs. 6.10(a, c, e, g, i). However, in the plates subjected to combined compression and negative in-plane shear loads, postbuckling response of plates with smaller size cutout is close to that of plates without cutouts. Although, critical buckling and first ply failure loads of FH_NC_$(+45/-45/0/90)_{2s}$ is higher than that of plates with smaller size cutouts regardless cutout shape, the load-deflection plots coincides at some or the other values of $w_{max}/$has shown in Figs. 6.10(b, d, f, h, j). In plate FH_EH1_$(+45/-45/0/90)_{2s}$, the postbuckling response is higher than plate without cutout after a certain value of deflection. Further, discussing about the effect of direction of shear load, plates subjected to

compressive loads combined with negative in-plane shear load outperform compared to positive shear load.

From Figs. 6.8, 6.9, and 6.10, it is observed that effect of composite layup sequences plays an important role in the buckling and postbuckling responses of functionally graded hybrid composite plates subjected to combined in-plane loads. Amongst the composite layups or fiber stacking sequences considered, the maximum critical buckling and first ply failure loads are observed in angle-ply laminates, i.e., fiber aligned in $(+45/-45)_{4s}$ direction and the minimum buckling and first ply failure loads are observed in cross ply laminates i.e., fiber aligned in $(0/90)_{4s}$ directions. The composite plates subjected to only in-plane shear loads (i.e., $N_x/N_{xy}=0$) has better performance irrespective of the direction of shear applied and presence of cutout.

6.4.3. Load interaction/Failure envelopes

The maximum buckling and failure loads are observed in FH plates without cutout and with diamond shaped small size cutout amidst all. Therefore, the effect of load ratios on composite plates without cutout and with small sized diamond shape cutout is shown in Figs. 6.11 to 6.13 and the corresponding interaction curves are shown from Figs. 6.14 to 6.16.

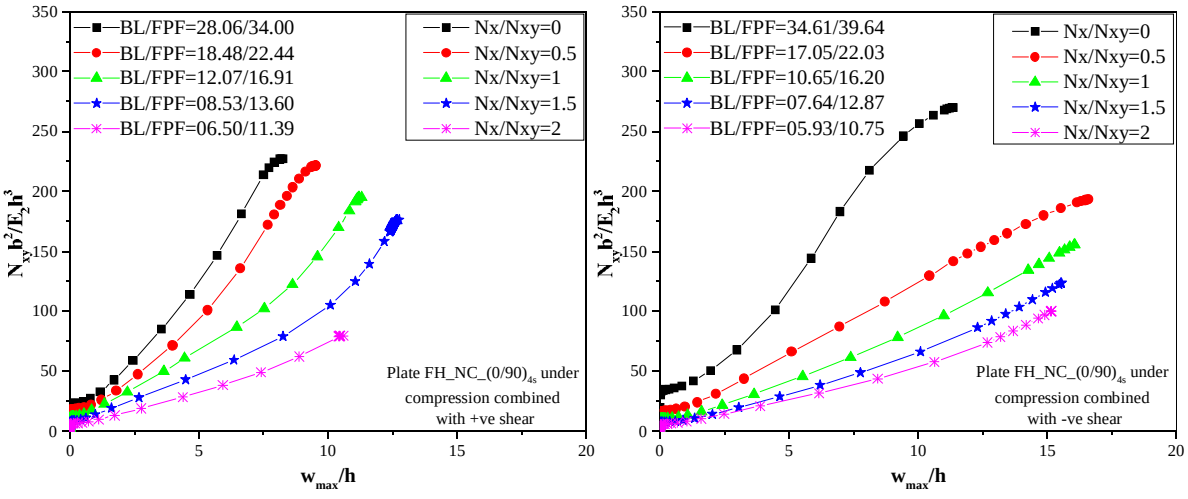

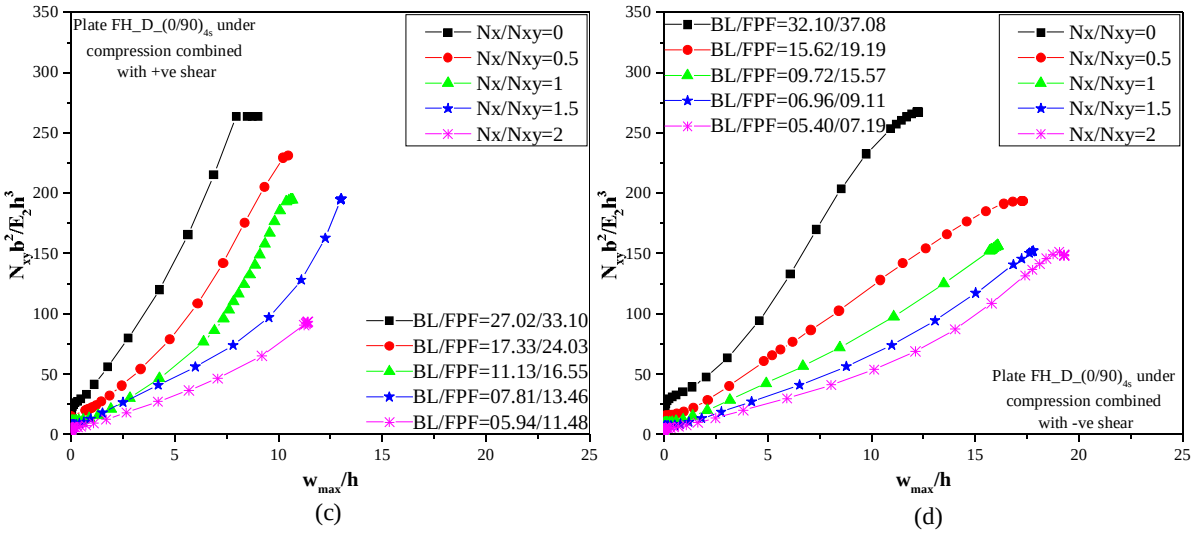

Fig. 6.11. Effect of load ratios on postbuckling response of functionally graded hybrid (FH) plates with fiber aligned in (0/90) direction under combined loads: (a) FH plate without cutout (NC) under uniaxial compressive load combined with +ve shear (b) FH plate without cutout (NC) under uniaxial compressive load combined with -ve shear (c) FH plate with diamond shaped (D) cutout under uniaxial compressive load combined with +ve shear (d) FH plate with diamond shaped (D) cutout under uniaxial compressive load combined with -ve shear

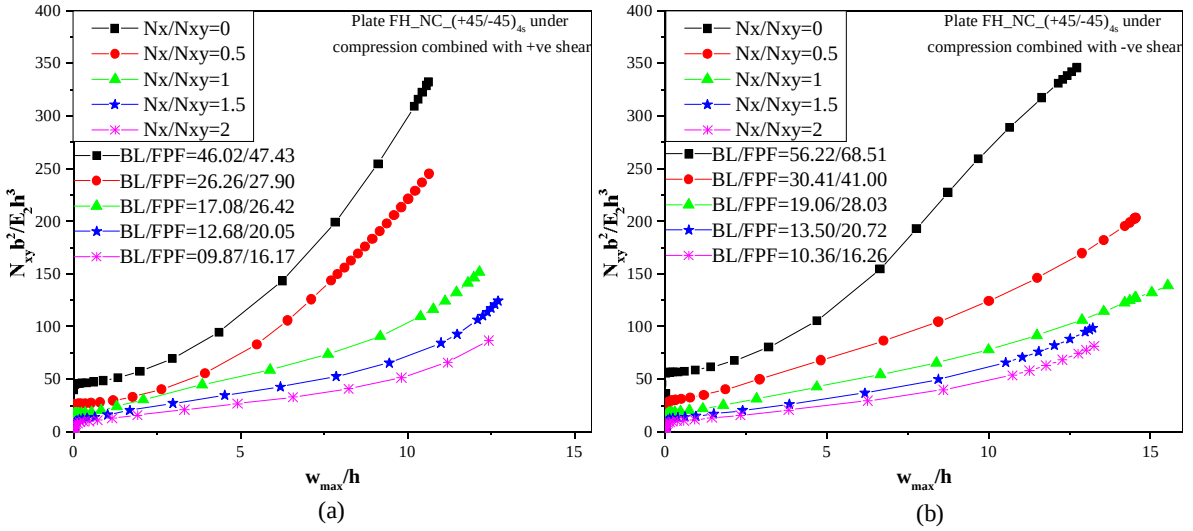

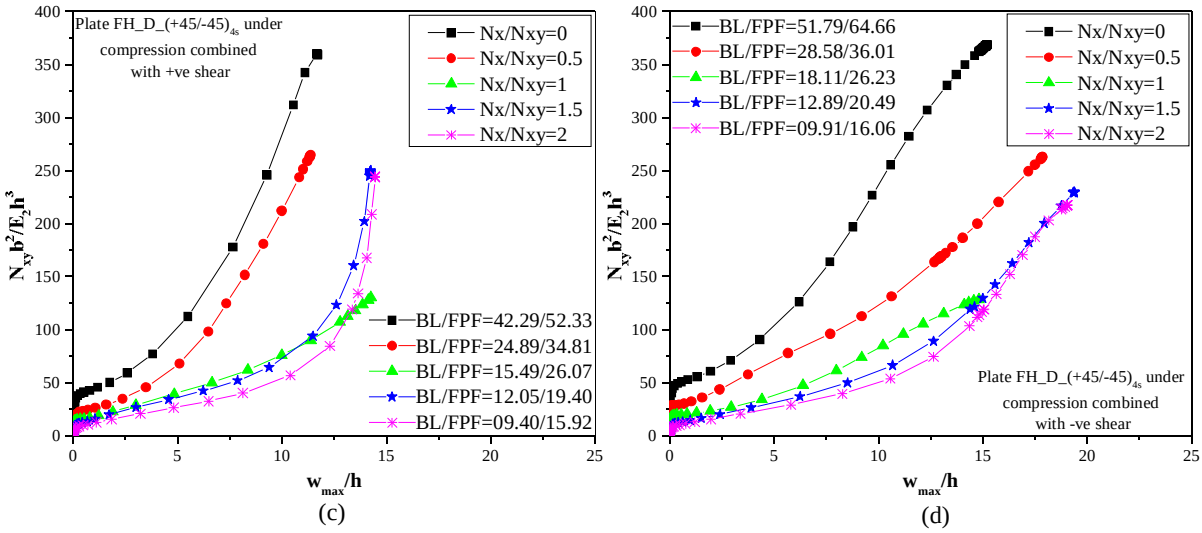

Fig. 6.12. Effect of load ratios on postbuckling response of functionally graded hybrid (FH) plates with fiber aligned in (+45/-45) direction under combined loads: (a) FH plate without cutout (NC) under uniaxial compressive load combined with +ve shear (b) FH plate without cutout (NC) under uniaxial compressive load combined with -ve shear (c) FH plate with diamond shaped (D) cutout under uniaxial compressive load combined with +ve shear (d) FH plate with diamond shaped (D) cutout under uniaxial compressive load combined with -ve shear

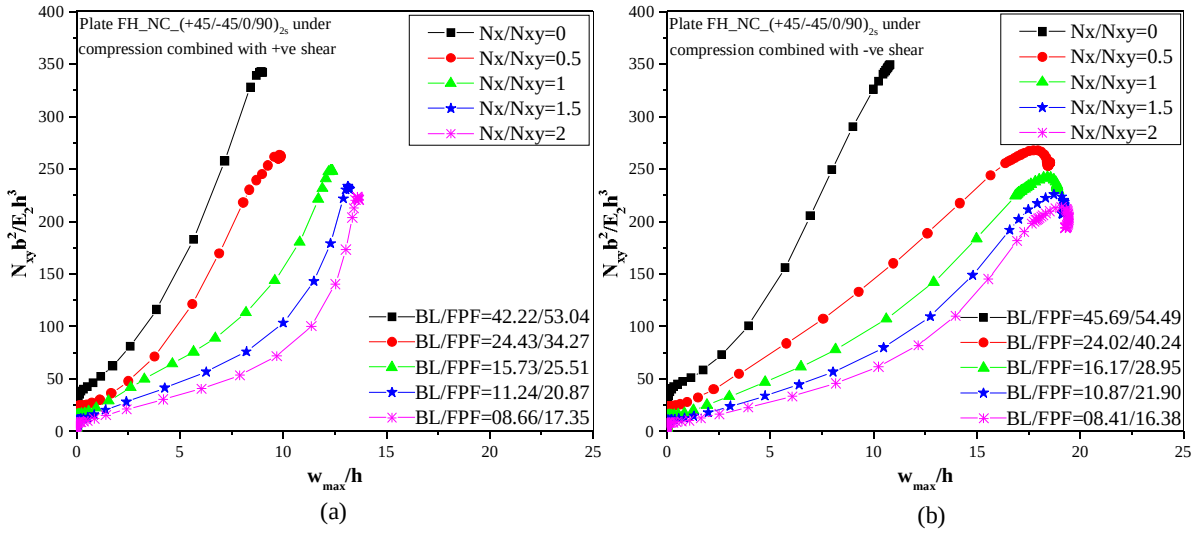

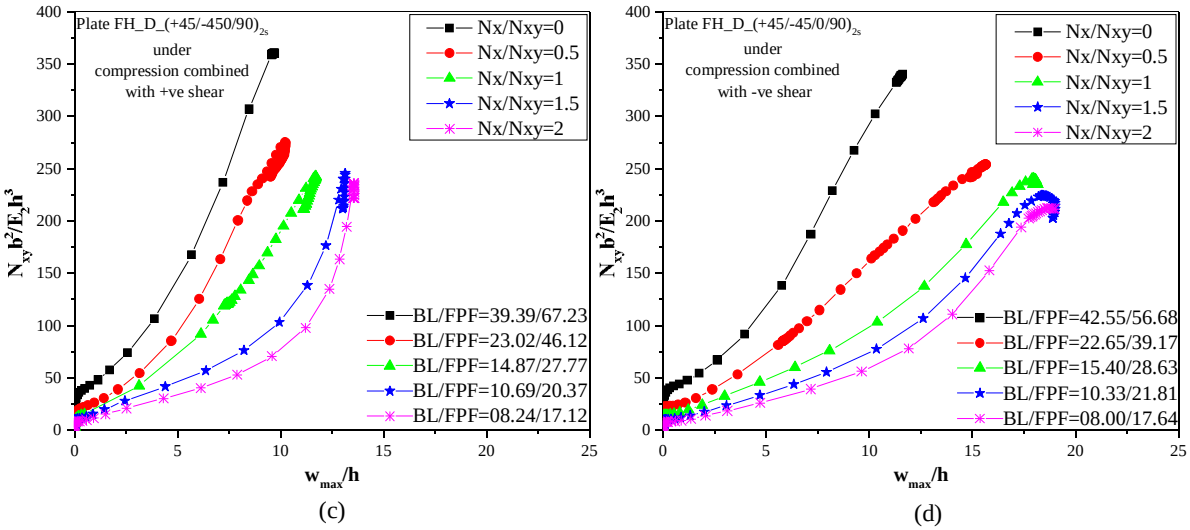

Fig. 6.13. Effect of load ratios on postbuckling response of functionally graded hybrid (FH) plates with fiber aligned in (+45/-45/0/90) direction under combined loads: (a) FH plate without cutout (NC) under uniaxial compressive load combined with +ve shear (b) FH plate without cutout (NC) under uniaxial compressive load combined with -ve shear (c) FH plate with diamond shaped (D) cutout under uniaxial compressive load combined with +ve shear (d) FH plate with diamond shaped (D) cutout under uniaxial compressive load combined with -ve shear

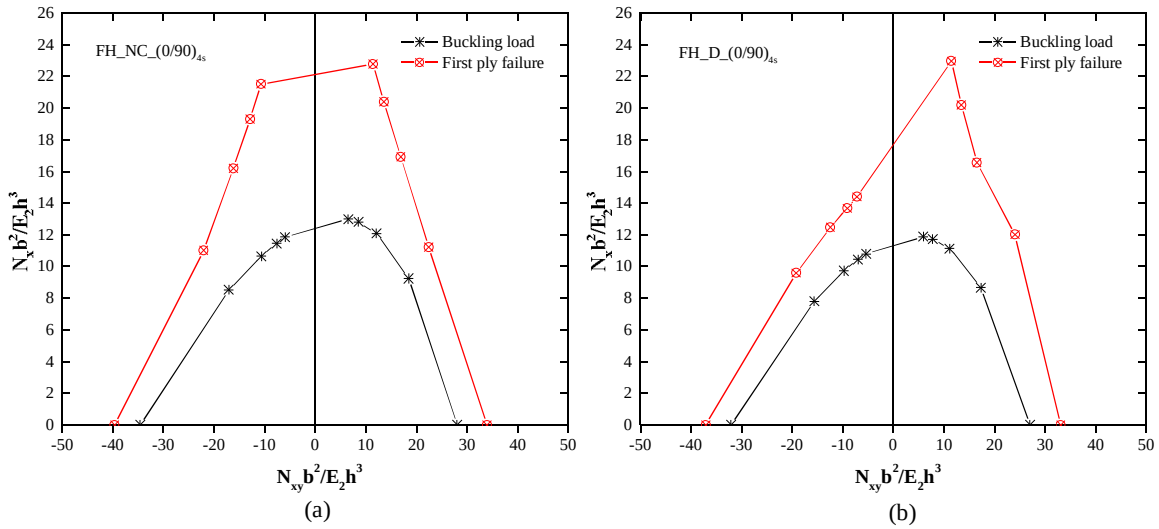

Fig. 6.14. Load interaction diagrams showing buckling load and first ply failure load for a square $(0/90)_{4s}$ functionally graded hybrid plate (a) Without cutout (b) Diamond shaped cutout

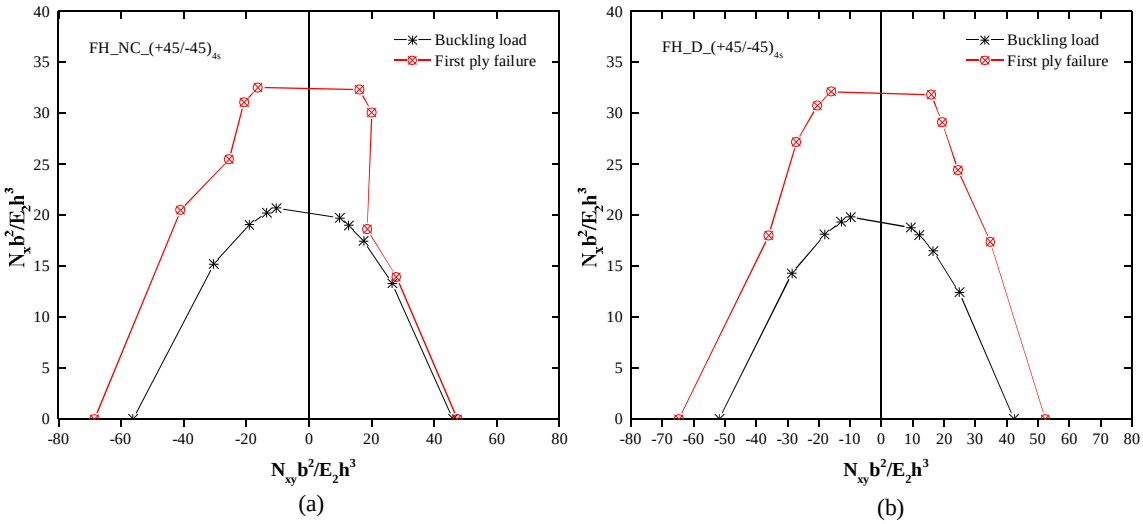

Fig. 6.15. Load interaction diagrams showing buckling load and first ply failure load for a square $(+45/-45)_{4s}$ functionally graded hybrid plate (a) Without cutout (b) Diamond shaped cutout

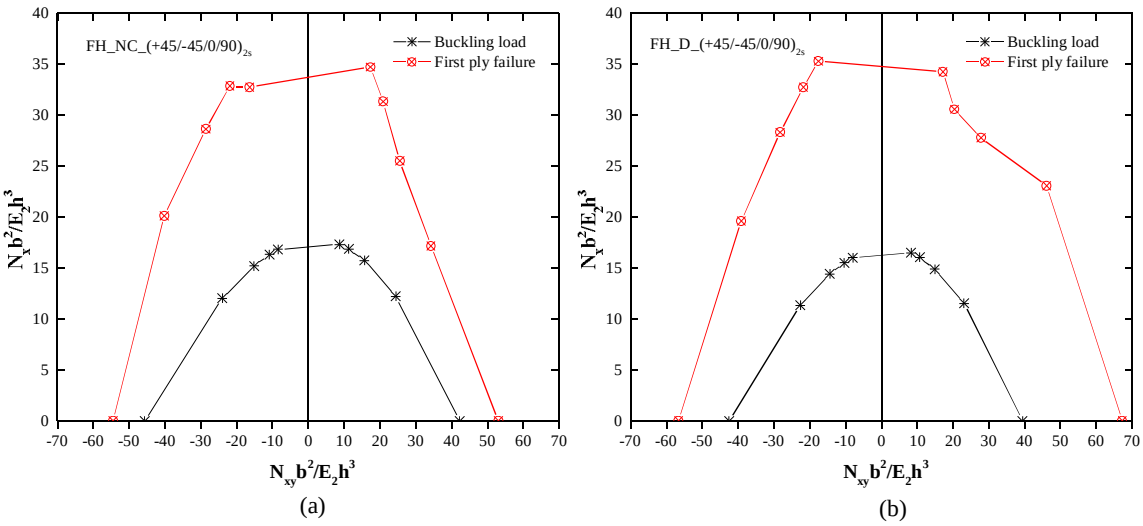

Fig. 6.16. Load interaction diagrams showing buckling load and first ply failure load for a square $(+45/-45/0/90)_{2s}$ functionally graded hybrid plate (a) Without cutout (b) Diamond shaped cutout

The ratio of uniaxial compressive load (N_x) to the in-plane shear loads (N_{xy}) are considered to investigate its effect on the load-deflection response. The N_x/N_{xy} ratios of 0, 0.5, 1, 1.5, and 2 are taken and the load-deflection responses are plotted as shown in Figs. 6.11, 6.12, and 6.13. The critical buckling and first ply failure load values are determined and depicted in the Tables 6.6 to 6.11. It has been observed that as the ratio of uniaxial compressive load (N_x) to the in-plane shear loads (N_{xy}) increases the buckling load, first ply failure load, ultimate failure load decreases with

overall postbuckling response. Load-interaction curves (Figs. 6.14 – 6.16) show the buckling load and first ply failure of FH plates without cutout and with a small size diamond shaped cutout with fiber stacked in $(0/90)_{4s}$, $(+45/-45)_{4s}$ and $(+45/-45/0/90)_{2s}$ sequences. It can be noted that buckling and first ply failure loads in the load-interaction diagram are not symmetric about the line $N_{xy}=0$. It is also observed that the buckling and failure load decreases as the FH plate is subjected to uniaxial compressive loading combined either with positive or negative in-plane shear load. It is also noted that effect of direction of in-plane shear is maximum in case of $(+45/-45)_{4s}$ stacking sequence where buckling as well as first ply failure loads are more for negative in-plane shear direction due to higher anisotropy. Effect of direction of in-plane shear is not much significant in case of $(0/90)_{4s}$ and $(+45/-45/0/90)_{2s}$ stacking sequences due to reduced anisotropy of these plates.

Table 6.6. Buckling and first ply failure loads of FH plate without cutout with stacking sequence $(0/90)_{4s}$ for various load ratios

Load ratios, N_x/N_{xy}	Compression combined with positive shear load BL(FPF)♣	Compression combined with negative shear load BL(FPF)♣
0	28.06(34.00)♣	34.61(39.64)
0.5	18.48(22.44)	17.05(22.03)
1	12.07(16.91)	10.65(16.20)
1.5	08.53(13.60)	07.64(12.87)
2	06.50(11.39)	05.93(10.75)

Note: All the values are non-dimensional (i.e., Nb^2/E_2h^3)
♣Buckling load (First ply Failure load)

Table 6.7. Buckling and first ply failure loads of FH plate with diamond shaped cutout with stacking sequence $(0/90)_{4s}$ for various load ratios

Load ratios, N_x/N_{xy}	Compression combined with positive Shear BL(FPF)♣	Compression combined with negative Shear BL(FPF)♣
0	27.02(33.10)♣	32.10(37.08)
0.5	17.33(24.03)	15.62(19.19)
1	11.13(16.55)	09.72(15.57)

1.5	07.81(13.46)	06.96(09.11)
2	05.94(11.48)	05.40(07.19)

Note: All the values are non-dimensional (i.e., Nb^2/E_2h^3)
♣Buckling load (First ply Failure load)

Table 6.8. Buckling and first ply failure loads of FH plate without cutout with stacking sequence $(+45/-45)_{4s}$ for various load ratios

Load ratios, N_x/N_{xy}	**Compression combined with positive Shear BL(FPF)♣**	**Compression combined with negative Shear BL(FPF)♣**
0	46.02(47.43)♣	56.22(68.51)
0.5	26.26(27.90)	30.41(41.00)
1	17.08(26.42)	19.06(28.03)
1.5	12.68(20.05)	13.50(20.72)
2	09.87(16.17)	10.36(16.26)

Note: All the values are non-dimensional (i.e., Nb^2/E_2h^3)
♣Buckling load (First ply Failure load)

Table 6.9. Buckling and first ply failure loads of FH plate with diamond shaped cutout with stacking sequence $(+45/-45)_{4s}$ for various load ratios

Load ratios, N_x/N_{xy}	**Compression combined with positive Shear BL(FPF)♣**	**Compression combined with negative Shear BL(FPF)♣**
0	42.29(52.33)♣	51.79(64.66)
0.5	24.89(34.81)	28.58(36.01)
1	15.49(26.07)	18.11(26.23)
1.5	12.05(19.40)	12.89(20.49)
2	09.40(15.92)	09.91(16.06)

Note: All the values are non-dimensional (i.e., Nb^2/E_2h^3)
♣Buckling load (First ply Failure load)

Table 6.10. Buckling and first ply failure loads of FH plate without cutout with stacking sequence $(+45/-45/0/90)_{2s}$ for various load ratios

Load ratios, N_x/N_{xy}	Compression combined with positive Shear BL(FPF)♣	Compression combined with negative Shear BL(FPF)♣
0	42.22(53.04)♣	45.69(54.49)
0.5	24.43(34.27)	24.02(40.24)
1	15.73(25.51)	16.17(28.95)
1.5	11.24(20.87)	10.87(21.90)
2	08.66(17.35)	08.41(16.38)

Note: All the values are non-dimensional (i.e., Nb^2/E_2h^3)
♣Buckling load (First ply Failure load)

Table 6.11. Buckling and first ply failure loads of FH plate with diamond shaped cutout with stacking sequence $(+45/-45/0/90)_{2s}$ for various load ratios

Load ratios, N_x/N_{xy}	Compression combined with positive Shear BL(FPF)♣	Compression combined with negative Shear BL(FPF)♣
0	39.39(67.23)♣	42.55(56.68)
0.5	23.02(46.12)	22.65(39.17)
1	14.87(27.77)	15.40(28.63)
1.5	10.69(20.37)	10.33(21.81)
2	08.24(17.12)	08.00(17.64)

Note: All the values are non-dimensional (i.e., Nb^2/E_2h^3)
♣Buckling load (First ply Failure load)

6.5. Concluding remarks

Based on the observations and results of the present study, some important conclusions are made.

1. Critical buckling, first ply failure and ultimate failure loads are higher in functionally graded hybrid composite plates subjected to in-plane shear loads with respect to uniaxial compressive loaded plates. However, the critical buckling, first ply failure and ultimate

failure loads of the similar plates are decreased when they are subjected to combined in-plane loads, i.e., in-plane uniaxial compression (N_x) and in-plane positive and negative shear loads (N_{xy}).

2. Functionally graded hybrid composite plates with smaller cutout size have better buckling and postbuckling responses under the application of combined loads irrespective of in-plane shear load directions, cutout shapes and layup sequences. The response of plate with small size cutout is very close to that of plate without cutout especially in case of combined compressive load with negative in-plane shear.
3. Composite plates with diamond shape cutout have best performance amongst the considered cutout shapes irrespective of the type of layup sequence and direction of shear loads.
4. FH plates under combined compressive load with negative in-plane shear with fiber aligned in (+45/-45) direction have higher critical buckling and first ply failure loads. Ultimate failure loads are higher in FH plates with fiber aligned in quasi isotropic fiber direction under combined compressive load with negative in-plane shear.
5. Effective utilization of plate stiffness until the ultimate load bearing capacity is seen in most of the FH plates subjected to combined compressive load with negative in-plane shear irrespective of stacking sequences.
6. As expected, increase in ratio of compressive load to in-plane shear load results in decrease in critical buckling, and postbuckling strengths of the composite laminates especially first ply failure loads.